Nazanin Jahani

Coupled Fluid Flow and Elasto-plastic Damage Analysis of Acid Stimulated Chalk Reservoirs

Thesis for the degree of Philosophiae Doctor

Trondheim, October 2015

Norwegian University of Science and Technology
Faculty of Engineering Science and Technology
Department of Engineering Design and Materials

NTNU
Kunnskap for en bedre verden

NTNU
Norwegian University of Science and Technology

Thesis for the degree of Philosophiae Doctor

Faculty of Engineering Science and Technology
Department of Engineering Design and Materials

ISBN 978-82-326-1102-7 (print)
ISBN 978-82-326-1103-4 (digital)
ISSN 1503-8181

Doctoral theses at NTNU, 2015:223

Printed by NTNU Grafisk senter

Preface

The present doctoral thesis is submitted to the Norwegian University of Science and Technology (NTNU) for the degree of Philosophiae Doctor (Ph.D.). The work has been carried out at Petrell AS in Trondheim and Department of Enginering Design and Materials (IPM) under the supervison of Dr. Geir Berge (Petrell AS), Associate Professor Bjørn Haugen (NTNU) and co-supervison of Professor Rune Martin Holt (NTNU and SINTEF Petroleum). The research has been funded by Petrell AS, The Research Council of Norway and Bp Norge AS.

Acknowledgments

I would like to present my sincere acknowledgment to people and institutions which directly or indirectly contributed to the achievement of this work. This work would be a lot more difficult to accomplish without their support and help.

My first thanks goes to Dr. Geir Berge, who has been my supervisor at Petrell AS, for believing in me and by giving me an opportunity to work at Petrell and later arranging my PhD project.

Many thanks to Associated Professor Bjørn Hauegn, my main supervisor of my PhD project for his continuous support and guidance toward my Ph.D study and related research.

I would like to give a special thanks to the manager of Petrell AS, Dr. Geir Langli, and office manager Linda Loktu for providing me the opportunity to do my PhD at Petrell AS and engaging me in lots of interesting activities.

Thanks to Professor Rune Martin Holt, my co-supervisor, for helpful discussions and guidances. His broad view of rock mechanic provided an important contribution to the work.

I would like to thank the rest of my thesis committee: Professor Eurpides Papamichos, Dr. Bård Bostrøm, and Professor Terje Rølvåg for their insightful comments and encouragement.

I have a great appreciation for the The Research Council of Norway for providing funding.

Thanks go to NTNU and the staff at department of Engineering Design and Materials for arranging this fellowship and their financial support toward my participation in two international conferences: Eurorock 2014 and 14IACMAG.

Sincere thanks to Bp Norge AS for their financial support.

I am also indebted to many people at ConocoPhillips, bp Norge , SINTEF petroleum, department of Structural Engineering at NTNU, with whom I have interacted during the course of my industrial PhD. Particularly, I would like to acknowledge Dr. Edvard Omdal, Kjetil Ormark, Dr. Roar Flateboe, Dr. Andreas Bauer and Professor Odd Sture Hopperstad for the many valuable discussions that helped me understand my research area better.

I consider it as a great honor to work with Dr. Bertold Plischke at ISAMGEO GmbH to implement the constitutive model of chalk into our in-house finite element software.

I would like to thank Dr. Mohammad Nassir at Taurus Reservoir Solutions Ltd for his guidance for implementing the fracture constitutive model.

I am grateful to Dr. Federico Zenith, for his recommendation and instructions in research and his useful guidances for writing academic papers, which have enabled me to assemble the thesis effectively.

A special acknowledgment goes to my office mate of many years Anders Granskogen Bjørnstad for the many helpful discussions and for all the fun we have had in the last five years. Thanks to my other colleagues: Dr. Zhiyong Huang for his contribution to development of the nonlinear finite element code. Torstein Hegge for his technical guidances and supports during years of code development, and his patient to answer my not very intelligent questions. Dr. Torgeir Ustad for many fruitful discussions. Silje kreken Almeland, Eirik Marthinsen, Ingunn Grip Fjær, Solveig Berthung, Øystein Olsen, Sebastian Roll and Roy Andre Midtgård, for enjoyable social activities.

I am grateful to Professor Dr. Werner Lehnert my supervisor in Jülich research center in Germany for his insightful comments and constructive criticisms, which taught me how to do research.

Many thanks to my main supervisors during my bachelor and master studies, Dr. Rambod Rayegan and Professor Kiumars Mazaheri for enlightening me the first glance of research.

I would like to thank one of my best teacher, Professor Hassan Khaleghi, who introduced me the field of numerical analysis.

Special thanks to my uncle Dr. Hossein Hosseinsadeh and my aunt Mansoureh Alamipour for their emotional support and their assistance to facilitate my residence in Europe.

I wish to acknowledge an especial friendship that began at Petrell AS with Mandana Amiri and Eirik Marthinsen and became ripe throughout my years in Trondheim.

Thanks to all my dear friends in Trondheim for providing me with enjoyable times.

I would like to express my gratitude to the most basic source of my life energy resides, my family: my two younger brothers Nariman Jahani and Saman Jahani and my parents Ahmad Jahani and Zahra Hosseinzadeh, who have been engaged in all activities in my life.

Abstract

Acid injection in a chalk oil reservoir can increase oil recovery by dissolving part of the fractured porous reservoir. Dissolution leads to the formation of conductive channels ("wormholes") that can increase the oil production. However, natural fractures in the reservoir affect the dissolution patterns by directing the flow potential along the fractures, and affect further acid treatments by creating a favorable flow path for the acid. Moreover, natural fractures influence the strength of both rock and wormholes. An eventual rock and wormhole failure would nullify the acid treatment.

Therefore, it is crucial to predict the contribution of natural fractures to dissolution patterns, the wormhole and reservoir strength and their failure threshold in order to design a successful acid treatment.

For this purpose, a continuum-based computational method is developed. The model includes flow in the porous chalk reservoir, flow in the wormhole, acid transport in the porous medium and dissolution of the fractured chalk, reversible and irreversible deformation of chalk and fractures, which are modeled with an equivalent elasto-plastic damage constitutive model. The coupling between the reservoir flow and the fractured chalk deformation is done by an explicit coupling method.

The results indicate that in a chalk core sample with a vertical fracture plane, which is orientated parallel to the plane between the inlet and the core, the injected acid has the best penetration depth through the core sample. However, the vertical fracture leads to high deviatoric stresses in the core, which can result in an earlier failure of the material, thus a negative effect on oil recovery. In addition, results show that the wormhole's walls failure risk is higher if the natural fractures are oriented along the wormhole; furthermore, natural fractures with larger dip angles and higher inclinations with respect to the wormhole increase the risk of the rock failure. The increased fluid production from the wormhole, which can be the result of the further acid treatments, develops irreversible behaviors of the rock and reduces the natural fracture asperity at the wormhole's tip, in addition to increasing the wormhole's wall deformation; this eventually leads to the wormhole's occlusion.

Contents

Chapter 1

Introduction

Oil consumption in the world is going to increase and oil supply declining rapidly and running out of cheap production. Therefore, there is a need to use a new technology to recover more oil. Recovery is extracting more oil and gas from existing reservoir. During drilling, natural pressure within the reservoir causes oil to flows out. This is primary recovery; however,the reservoir's pressure declines and extraction of oil due to the initial pressure stops, but two third of oil is still underground, thus the secondary recovery is used in the depleted reservoir by utilizing different technologies such as installing pumps or injection of water and gas into the well. In low permeability and porosity reservoirs, oil is trapped on the rock and is unable to be extracted by the initial drilling. In this case, well stimulation techniques such as fracturing is used to increase the permeability of the rock. Two ways of well stimulation are fracturing and matrix acidizing. In fracturing stimulation, fluid is injected in higher pressure than the reservoir pressure, which leads to opening of new channels. The injected fluid can be oil water or acid. In the matrix acidizing, acid is injected at a lower pressure than the required pressure for the fracturing method. In this method acid reacts with the rock, dissolves portion of the rock and open up the existing spaces that leads to an less restrictive pattern for oil to flow. This allows more fluid to drain to the well-bore and enhance the oil recovery.

The reservoir acidizing is almost as old as the oil reservoir drilling. The well stimulation by hydrochloric acid [HCI] was first attempted in 1896 in Ohio oil company, but acid corroded well casing, and this technique didn't get used again for 30 years. In 1932, Dr John Grebe, from Dow company found out that arsenic inhibited the action of HCI on metal, and matrix acidizing is reborn. Three years after that Halliburton company started developing commercial acidizing [14].

Well stimulation by the acid is getting increasingly important to make drilling more economical. However, it is important to know that rock dissolution by acid does not always improve the oil productivity from the reservoir.

Various factors such as the acid injection rate, diffusion coefficient of the acid species, concentration of acid, temperature and heterogeneity of the formation influence the dissolution pattern and affects the production rate and stability of the well-bore. These dissolution patterns are divided to face dissolution, wormholing, and uniform dissolution. If the large portion close to the well is completely dissolved, it is called face dissolution; conversely, if too much of the chalk is removed by dissolution, it is called uniform dissolution. There is an optimum condition at which long channels will be formed. Acid etches the wall of the pores, opens their walls and creates channels that go through the chalk like a worm, hence the name "wormhole". Creation of wormhole pattern increases oil production, because it has the best penetration depth for the same volume of injected acid [20, 57]. Figure 1.1 illustrates a wormhole patterns from the experimental works has been done by Bauer et al. [3].

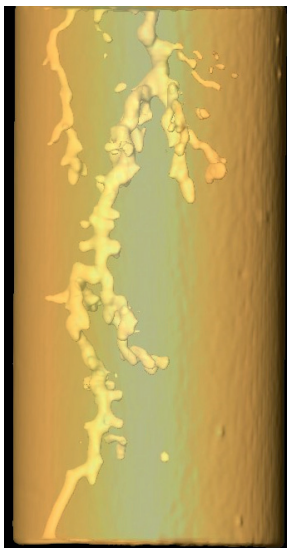

Figure 1.1: Radiographs of wormholes formed during the dissolution of chalk [3].

Counter to the increasing oil production and oil recovery due to the acidizing, is the increased risk of rock breaking down. The stress states of the rock is changed in the area where the wormholes and fractures are formed and this influences the resulting effectiveness of the acid treatment.

From the above discussion, in order to have a successful acid fracturing, it is important to investigate the effect of the presence of fractures and wormholes on the rock strength and consequently on the oil production.

1.1 Objective

In order to understand the physical behavior of the stimulation process, we will use computer simulation, which is cheaper, more flexible and faster than experimental works. The objective of this thesis is:

1. Presenting a simulation approach that treats the subject efficiently and in accordance with physics.
2. Predicting risk of the rock failure due to the presence of the wormhole and fractures.
3. Understanding the interaction between the acid injection and the formed dissolution pattern and the stress states of the rock.

1.2 Method

The case study simulated in this thesis is a core sample representing the near well bore area of the chalk reservoir. The core sample includes pre-existing fractures. These fractures can be natural fractures in the rock or fractures created by hydraulic fracturing or other stimulation treatments such as previous acid injection. The fluid flow and acid transport in the core sample is modeled by the flow in the fractured porous media on a Darcy scale. The prediction of the rock failure, wormhole and damage of the fractures has been done by using a continuum approach and applying an equivalent constitutive model, which considers both chalk and fracture deformation.

The thesis is divided into three main parts:

1. The fluid flow model including the acid transport and the rock dissolution, which is described in Chapters 2 and 3.
2. The geomechanical model including both reversible and irreversible behaviors of the rock and fractures, which is explained in Chapter 4.
3. The coupling method between the two models is presented in Chapter 5.

In Chapter 6 a brief discussion of the numerical methods to solve equations representing the physical behavior of the model is described .

Chapter 2

Fluid Flow in the Fractured Rock

Carbonate reservoirs as a source of water and oil are fractured system. The fractured reservoirs are divided in two types: fractured reservoirs of single porosity and fractured reservoirs of double porosity. In both cases the reservoir consists of fractures surrounding the block or matrix. In a single porosity fractured reservoir, the matrix is impervious and the total porosity is considered as only the matrix porosity, however in double porosity both matrix and fractures porosities are considered [23]. In this thesis the theory of a single porosity is applied.

2.1 Flow in the Single Porosity Fractured Reservoir

In single porosity reservoirs, flow takes place only through the network of fractures. The flow can be formulated through the continuum approach. A volume block with discontinuous fractures is replacing with a continuum block with equivalent properties. The equation of flow can be formulated by partial differential equations, Flow through the fracture is primarily laminar and the equation of motion is represented by Darcy's law.

2.1.1 Darcy Velocity

From Darcy's law, the flow discharge through the network of fractures is proportional to the hydraulic gradient and hydraulic conductivity by the following equation,

$$\boldsymbol{Q}_l = -A\mathsf{K}\nabla h \tag{2.1}$$

where $\boldsymbol{Q}_l$ is the flow discharge vector, A is the cross sectional area of the rock, K is the second rank tensor, and ∇h is the hydraulic gradient vector. By neglecting

the gravity effect, the hydraulic head gradient is replaced by total pressure drop:

$$\nabla h = \frac{\nabla p}{\rho g} \tag{2.2}$$

In Equation (2.1), K represents the hydraulic conductivity of the heterogeneous porous medium and is related to a permeability tensor by a scalar factor as follows,

$$\mathsf{K} = \rho g \frac{\mathsf{k}}{\mu} \tag{2.3}$$

The scalar factor is the fluid physical properties and includes the dynamic viscosity μ, the fluid density ρ, and the acceleration of gravity g. k is the permeability tensor and represents the directional resistances of the porous media to the flow.

Darcy velocity vector is obtained by dividing Equation (2.1) over the cross section A and substituting Equation (2.2) and (2.3) into Equation (2.1) as:

$$\boldsymbol{q} = -\frac{\mathsf{k}}{\mu}\nabla p = -\mathsf{k}\boldsymbol{\tau} \tag{2.4}$$

where ∇p is the pressure gradient vector. The fluid velocity vector $\boldsymbol{U}$ is related to the Darcy flux $\boldsymbol{q}$ by porosity (φ) as:

$$\boldsymbol{U} = \frac{\boldsymbol{q}}{\varphi} \tag{2.5}$$

2.1.2 Flow through an Individual Fracture

Flow through an individual fracture is modeled by the flow through the two parallel plates with a narrow space between [23]. This is governed by the Navier-Stokes equation by assuming a small Reynolds number,

$$\boldsymbol{U} = -\frac{w_f^2}{12\mu}\boldsymbol{\tau}_p \tag{2.6}$$

where w_f is the distance between two parallel plates or the fracture aperture. $\boldsymbol{\tau}_p$ is the projection of the pressure gradient parallel with the fracture. According to the vector difference, the pressure gradient is split into two components, one in the direction of the fracture plane,$\boldsymbol{\tau}_p$, and the other in the normal direction,$\boldsymbol{\tau}_n$, with $\hat{n}$ as unit vector.

$$\boldsymbol{\tau}_p = \boldsymbol{\tau} - \boldsymbol{\tau}_n \tag{2.7}$$

$$\boldsymbol{\tau}_p = \boldsymbol{\tau} - (\boldsymbol{\tau} \cdot \hat{n})\hat{n} \tag{2.8}$$

on substitution, the velocity given by Equation (2.6) becomes,

$$\boldsymbol{U} = -\frac{w_f^2}{12\mu}(\boldsymbol{\tau} - (\boldsymbol{\tau} \cdot \hat{n})\hat{n}) \tag{2.9}$$

or alternatively

$$\boldsymbol{U} = -\frac{w_f^2}{12\mu}(\delta_{ij} - n_i\, n_j)\boldsymbol{\tau} \tag{2.10}$$

by substituting Equation 2.10 into Equation (2.5) and by comparison with Equation (2.4), the permeability tensor in Equation (2.4) is defined as:

$$\mathsf{k} = \varphi\frac{w_f^2}{12\mu}(\delta_{ij} - n_i\, n_j)\mathbf{i}_i\mathbf{i}_j \tag{2.11}$$

Permeability in Equation(2.11) can be written a product of two components, the permeability scalar and the unit permeability tensor as follows,

$$\mathsf{k} = |k|[\mathsf{k}] \tag{2.12}$$

The permeability scalar can be defined as,

$$|k| = \varphi\frac{w_f^2}{12\mu} \tag{2.13}$$

The unit permeability tensor $[\mathsf{k}]$ is defined in a compact form,

$$[\mathsf{k}] = (\delta_{ij} - n_i\, n_j)\mathbf{i}_i\mathbf{i}_j \tag{2.14}$$

where δ_{ij} is the Kronecker delta; n_i and n_j are components of the normal vector to the fracture plane $\hat{n}$. i and j stand for the orthogonal local references axes x', y' and z' on the fracture plane. In order to evaluate the flow discharge from Darcy law in Equation (2.1), the hydraulic conductivity tensor is obtained by multiplying the permeability tensor by the cross section area perpendicular to flow ($2w_f \times H$); Hydraulic conductivity tensor becomes,

$$\mathsf{K} = -\frac{2\varphi H}{3\mu}\, w_f^3\, (\delta_{ij} - n_i\, n_j)\mathbf{i}_i\mathbf{i}_j \tag{2.15}$$

Fracture Orientation

The orientation defines a single fracture plane in space. In Geology, a planar surface is commonly defined in terms of strike line and dip line. The strike line of a planar feature, is the line representing the intersection of that fracture with an imaginary

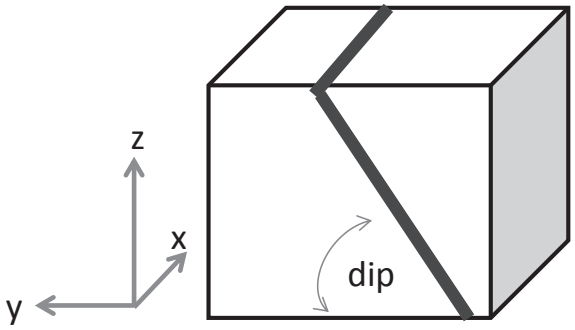

Figure 2.1: An illustration of a Fracture plane with dip angle d and azimuth 90°

horizontal plane. The angle between the strike line and a reference vector, (y) is called the azimuth. The inclination angle between the inclined fracture and the horizon is the dip angle d. A fracture plane and its orientation is illustrated in figure (2.1). In this work the fracture plane is defined with their local coordinate system with orthogonal axes of x', y' and z', the vector normal to the fracture plane is in x' direction, The block coordinate axes are x,y and z, where z is the vertical direction and x and y axes are on the horizontal plane.

2.1.3 Continuity Equation

In Darcy equation, there is two unknown parameters, the velocity and pressure gradient vectors. The velocity vector can be defined by using the mass continuity equation, which is based on the principle of conservation of mass, and indicates that the rate at which mass enters a system is equal to the rate at which mass leaves the system. The continuity equation is described as follows.

$$\frac{\partial \rho \varphi}{\partial t} + \nabla \cdot \boldsymbol{U} = q_s \tag{2.16}$$

where q_s is the source and sink term, describing reservoir withdrawal or injection, and φ represent porosity of the rock. The continuity equation leads to the Equation (2.17) for in-compressible flow by making an assumption that the process is in steady-state and there is no sink and source term.

$$\nabla \cdot \boldsymbol{U} = 0 \tag{2.17}$$

2.1.4 Species Transport Equation

The transport equation is derived by balancing all mass fluxes across the system. Here, convection and dispersion determine the transport process of fluid in the

porous media. The transport equation is applied to all species in the system.

$$\varphi \frac{\partial C}{\partial t} + \boldsymbol{U} \cdot \nabla C - \nabla \cdot (\varphi \mathsf{D_e} \cdot \nabla C) - q_m = 0 \tag{2.18}$$

The first three terms in the equation represent accumulation, convection and dispersion of the material, respectively. The forth term is defined as a sink or source term. C is the species concentration, $\mathsf{D_e}$ is the dispersion. In this work the effect of heterogeneity of the porous media for defining the dispersion tensor is not considered and hence $\mathsf{D_e} = D_e \mathbf{I}$.

Chapter 3

Acid Injection into the Fractured Reservoir

As it was mentioned in the Introduction, acid injection is used for stimulation of carbonate reservoirs to increase the rock permeability and porosity. The process of carbonate reservoir dissolution is discussing in the following.

3.1 Model for Rock Dissolution

Acid flows by convection into pore spaces. The acid molecules are transferred to the surface of pores and reacts with the rock and the reaction products transfer back to the bulk of the flowing acid. As a result of the reaction, porosity evolves and creates an easier path for the flow leading to increased permeability. However, the presence of natural fractures or medium heterogeneity leads to an uneven dissolution. The fractured parts of the medium with higher permeability attract more acid, which further dissolves the natural fractures, creating channels and travel ahead of the front. Heterogeneity is required for the channel formation. However, according to experimental studies [20, 21], a highly branched channel or "wormhole" is required to increase in permeability and leading to favorable reservoir stimulation. The channel structure depends on relative magnitudes of convection, dispersion, and reaction in the medium [58], which again depend on the local pore structure, local velocity of the fluid, local diffusion and local reaction rate. If the reaction is slow, the process is considered in a reaction-rate controlled regime, and the result is more uniform acid distribution. However, if the reaction is very fast compared to the mass transfer, the process is known as being in the mass-transfer controlled regime. The mass transfer and reaction parameters are obtained from the pore scale modeling. Therefore, the rock dissolution phenomena is a coupling between

processes at two length scales: Darcy scale and pore scales. Since, the channel structure is not the objective of this work, the pore scale parameters obtained from studies of Golfier et al. [24] and are inputs to the Darcy scale.

A mathematical description of acid transport in fractured porous medium and dissolution process is presented by Golfier et al. [25] by considering the following assumptions.

1. The reaction products, which transfer back to the bulk, are very small thus it is assumed they do not change their total fluid mass.

2. The interface shape changes are slow, hence the dissolution does not change the mass flux; continuity equation is considered in steady-state if there is not any other sink and source term.

3. This model is considered as a mass transfer controlled regime; the reaction is very fast and the acid concentration at the fluid-solid phase is negligible.

The velocity and pressure field for acid flow is calculated from the equations in the flow model, which are described in the previous section. The acid concentration at each point of the reservoir is evaluated from the transport equation.

3.1.1 Acid Transport Equation

The transport equation for acid in the porous media approximated as:

$$\varphi \frac{\partial C_a}{\partial t} + \boldsymbol{U} \cdot \nabla C_a = \nabla \cdot (\varphi \mathsf{D_e} \cdot \nabla C_a) - \alpha_c(C_a) \tag{3.1}$$

The forth term of the Equation (3.1) is defined as a sink or the acid consumption term and describes the depletion of acid due to the reaction. α_c is the local mass transfer coefficient. The detailed information are available in [25, 62].

3.1.2 Rock Dissolution

The amount of solid dissolved, which causes porosity evolution, is equivalent to the amount of acid consumed; The evolution of the porosity field is defined by using the stoichmietry of the reaction written in equation(3.2).

$$\frac{\partial \varphi}{\partial t} = \frac{\beta \, \alpha_c C_a}{\rho_R} \tag{3.2}$$

where ρ_R is the rock density, β represents the stoechiometric coefficient of the chemical reaction. The resulting acid concentration profile from equation(3.1) is used to solve the dissolution equation to find the new porosity field.

Chapter 4

Mechanical Behavior of the Fractured Chalk

As it was mentioned, acid injection into a carbonate reservoir may increase the reservoir permeability and leads to reservoir productivity enhancement. However, the injected acid influences the physical behavior of the carbonate reservoirs by changing some parameters such as the heterogeneity of the media due to the fractures formation or the rock dissolution, and by changing the fluid pressure in the porous media. Since carbonate reservoirs such as chalk are a group of highly deformable geo-materials with significant nonlinearity in their constitutive behavior, acid injection may lead to reservoir failure due to the change of their constitute behavior.

In order to model the constitute behavior of the fractured chalk, a coupled constitutive model, which can incorporate both chalk and fracture deformation is required. The presented model in this work is divided to three parts: intact chalk constitutive model, fracture constitutive model, and a coupled model for the fractured chalk. Both intact chalk and fracture display reversible and irreversible deformations. The linear elastic model represents the reversible deformation of the chalk and the fracture. The irreversible deformation of the chalk is modeled by the theory of nonlinear plasticity, and nonlinear damage theory is used to represent the irreversible deformation of the fracture. Lastly a coupled elasto-plastic-damage model is developed to demonstrate the constitute behavior of the fractured chalk.

4.1 Linear Elastic Models

The constitutive behavior is expressed mathematically and relates stress tensors to strain tensor in the following form. The constitutive relationship is written on

matrix form, and hence stress and strain tensors are written as (matrix) vectors. Because of this, the stress and strain states are often referred to as "vectors" in the following sections.

4.1.1 Linear Constitutive Model for the Intact Chalk

The linear stress-strain relation of the intact chalk (without discontinues fractures) is written as:

$$\boldsymbol{\sigma} = D_I \boldsymbol{\varepsilon}_I^e \tag{4.1}$$

where $\boldsymbol{\sigma}$ is the stress vector, $\boldsymbol{\varepsilon}_I^e$ is the elastic strain incremental vector. For the linear elastic chalk, the constitutive matrix, D_I and takes the following form;

$$\mathsf{D}_I = \frac{E}{1+\nu}\begin{bmatrix} 1-\nu & \nu & \nu & 0 & 0 & 0 \\ \nu & 1-\nu & \nu & 0 & 0 & 0 \\ \nu & \nu & 1-\nu & 0 & 0 & 0 \\ 0 & 0 & 0 & 0.5-\nu & 0 & 0 \\ 0 & 0 & 0 & 0 & 0.5-\nu & 0 \\ 0 & 0 & 0 & 0 & 0 & 0.5-\nu \end{bmatrix} \tag{4.2}$$

where E and ν are Young's Modulus and Poisson's ratio, respectively. The linear constitutive model of intact chalk is assumed as an isotropic and symmetric model.

4.1.2 Linear Constitutive Model for the Fracture Plane

The fracture is modeled as a 2-D plane. The linear stress-strain relation of the single fracture is written as,

$$\boldsymbol{\varepsilon}'^{d} = \mathsf{F}_J \boldsymbol{\sigma}' \tag{4.3}$$

where $\boldsymbol{\sigma}$ is the stress vector at the local coordinate system, $\boldsymbol{\varepsilon}'^{d}$ is the elastic strain vector of the fracture in its local coordinate system. F_J is the elastic compliance matrix of the single fracture plane in the local coordinate system and takes the following form:

$$\mathsf{F}_J = \begin{bmatrix} k_n^{-1} & 0 & 0 \\ 0 & k_s^{-1} & 0 \\ 0 & 0 & k_t^{-1} \end{bmatrix} \tag{4.4}$$

k_n is the stiffness normal to the fracture plane, and k_s and k_t are the shear stiffnesses of the fracture plane in two orthogonal directions in the local coordinates of the fracture plane [52].

4.2 Elasto-plastic Model

If some parts of the intact chalk in response to applied load is undergoing irreversible deformation,the material behavior is elasto-plastic. Because the elasto-plastic behavior of the material depends on the stress history of the material, the constitutive relations are expressed in incremental form as:

$$\Delta\boldsymbol{\sigma} = \mathsf{D}^{ep}\Delta\boldsymbol{\varepsilon} \tag{4.5}$$

To build a constitutive model for the chalk, the following concepts and principals are required;

Strain Additive

The total incremental strain can be split additively into elastic and plastic part.

$$\Delta\boldsymbol{\varepsilon} = \Delta\boldsymbol{\varepsilon}^{e} + \Delta\boldsymbol{\varepsilon}^{p} \tag{4.6}$$

Yield Surface

The material have certain admissible stress-strain states, at which stress versus strain can not reach beyond this state. The boundary between admissible and inadmissible stress state regions is defined by a surface called yield surface. Material which lies under the yield surface is called elastic, whereas on the yield surface the material have elasto-plastic behavior. The surface is a function of the stress state, $\boldsymbol{\sigma}$, and its size changes as a function of the internal parameters $\boldsymbol{\eta}$, which can be related to hardening or softening parameters. Hardening and softening parameters are related to the magnitude of plastic strain or plastic work.

The magnitude of a yield function F is used to identify the type of the material behavior. If $F(\boldsymbol{\sigma}, \boldsymbol{\eta}) < 0$, the material is purely elastic, and the material displays plastic behavior if $F(\boldsymbol{\sigma}, \boldsymbol{\eta}) = 0$, and $F(\boldsymbol{\sigma}, \boldsymbol{\eta}) > 0$ is an inadmissible situation. In this work, the yield function is calculated from the stress invariant quantities instead of stress vectors. Stress invariant quantities are useful because they are independent of the reference axes. The various invariants, which are used here, are listed in the following section.

Stress and Strain Invariant

The invariants defined for 3-D space are as follows,

1. Mean stress, p_m

$$p_m = \frac{1}{3}(\sigma_{xx} + \sigma_{yy} + \sigma_{xx}) \tag{4.7}$$

2. Deviatoric stress, J

$$J = \sqrt{3J_2} \tag{4.8}$$

where J_2 is the 2nd invariant of deviatoric stress,

$$J_2 = \frac{1}{2}[S_x^2 + S_y^2 + S_z^2] + \sigma_{xy}^2 + \sigma_{yz}^2 + \sigma_{zx}^2 \tag{4.9}$$

where, $S_x = \sigma_{xx} - p_m$, $S_x = \sigma_{xx} - p_m$, $S_x = \sigma_{xx} - p_m$.
Often $\sqrt{J_2}$ is used as a parameter of the yield function.

3. Lode angle, θ
The load angle θ is defined via

$$\sin(3\theta) = \frac{3\sqrt{3}}{2}\frac{J_3}{J_2\sqrt{J_2}} \tag{4.10}$$

J_3 is the third invariant of deviatoric stress,

$$J_3 = S_x S_y S_z + 2\sigma_{xy}\sigma_{yz}\sigma_{zx} - S_x\sigma_{yz}^2 - S_y\sigma_{zx}^2 - S_z\sigma_{xy}^2 \tag{4.11}$$

Plastic Flow Rule

In order to define the direction of plastic strain regarding to the imposed stress, a flow rule is defined. From the principal of maximum plastic dissipation and Kuhn-Tucker optimality condition [47], the flow rule can be expressed as follow,

$$\Delta\boldsymbol{\varepsilon}^p = \gamma^p \frac{\partial Q^p}{\partial \boldsymbol{\sigma}} \tag{4.12}$$

where $\Delta\boldsymbol{\varepsilon}^p$ is the incremental plastic strain vector, Q^p is the plastic potential function, and γ^p is a plastic scalar multiplier, which is a non-negative value. If the potential function is equal with the yield function, the plasticity model is called the associated; otherwise, non-associated [30].

4.2.1 The Elasto-plastic constitutive model of Chalk: The ISAMGEO Chalk model

Chalk behaves as a frictional material and its ultimate strength is defined with respect to the shear failure, in which the grains of material slide relative to each other. However, shear failure is not the only failure mechanism that may occurs in chalk; chalk is a high porous material and under a compressive loading an irreversible decreasing in pore volume is observed, which is described as pore collapse yielding. In this work, the constitutive model of the present mechanical behavior of chalk is

based on the ISAMGEO chalk model, which has been developed by Plischke [60]. The chalk model includes two independent yields mechanisms: shear failure and pore collapse. The shear failure have priority over the pore collapse. However, another failure mechanism in which the chalk grains pull apart is also observed experimentally, and is often called tensile failure. In this work we neglect the rock failure due to the tensile.

1. Shear Failure: The yield function is straight line in stress invariant (J, P_m) space defined by the Mohr-Coloumb function as follows,

$$F^p = \sqrt{J_2}\left\{\cos(\theta) - \frac{\sin(\phi)\ \sin(\theta)}{\sqrt{3}} - \zeta\ [2\cos(2\theta) - 1]\right\} + \\ - \left[p_m\ \sin(\phi) + c\ \cos(\phi_{\text{peak}})\right] \quad (4.13)$$

and the potential function is expressed as,

$$Q^p = \sqrt{J_2}\left\{\cos(\theta) - \frac{\sin(\psi)\ \sin(\theta)}{\sqrt{3}} - \zeta\ [2\cos(2\theta) - 1]\right\} + \\ - \left[p_m\ \sin(\psi) + c\ \cos(\psi_{\text{peak}})\right] \quad (4.14)$$

where, ζ scales the impact of the intermediate principal stress. ϕ is the friction angle and c is the cohesion, which are both varying due to hardening and softening. Note that the plastic potential Q^p is described by the same function as the yield. However, the friction angle ϕ is replaced by the dilatancy angle ψ. In order to have a realistic description of the volumetric plastic strain changes, a non-associated flow rule is used.

Chalk properties such as cohesion and friction vary during loading, which harden or soften the Mohr-Coloumb yield function. Hardening of the yield surface is applied to the model by increasing the friction angle before shear strength reaches the peak stress. After reaching the peak stress, the material experiences pronounced softening by decreasing cohesion and friction angle. For the dilatancy angle ψ, the hardening and softening are the same as for the friction angle ϕ. Increase of the friction angle from ϕ_{ini} to ϕ_{peak} is described by the following relation.

$$\phi = \phi_{ini} + \frac{(\phi_{peak} - \phi_{ini})\sqrt{2\,\varepsilon_{pl}\,\varepsilon_{pl}^{peak} - (\varepsilon_{pl}^{peak})^2}}{\varepsilon_{pl}^{peak}} \quad (4.15)$$

After reaching the peak strength (specified as: $\varepsilon_{pl} = \varepsilon_{pl}^{peak}$), there is an exponential decline to the residual values, ϕ_{res}.

$$\phi = (\phi_{peak} - \phi_{res})\, e^{\Upsilon(\varepsilon_{pl} - \varepsilon_{peak})} + \phi_{res} \quad (4.16)$$

Cohesion c is assumed to be constant as the initial value c_{ini}, until the peak strength is reached. Cohesion then decline linearly until the residual cohesion c_{res} is reached.

$$c = c_{ini} - \eta\,(\varepsilon_{pl} - \varepsilon_{pl}^{peak}) \tag{4.17}$$

where Υ and η are the hardening and softening parameters.

Equivalent plastic strain, ε_{pl}, is defined as:

$$\varepsilon_{pl} = \sqrt{2\,(\varepsilon_{xx,pl} - \frac{\varepsilon_{v,pl}}{3})^2 + (\varepsilon_{yy,pl} - \frac{\varepsilon_{v,pl}}{3})^2 + (\varepsilon_{zz,pl} - \frac{\varepsilon_{v,pl}}{3})^2 + \varepsilon_{xy,pl}^2 + \varepsilon_{yz,pl}^2 + \varepsilon_{zx,pl}^2} \tag{4.18}$$

where, $\varepsilon_{v,pl}$ is the volumetric plastic strain.

2. Pore Collapse: The yield surface for pore collapse is defined by an ellipse in $J - p_m$ space, and the flow rule is assumed as an associated plastic flow. The pore collapse yield function is expresses as,

$$F^p = 3\,\sqrt{J_2}^2 + M^2\,(p_m^2 - p_m\,p_{cc}) \tag{4.19}$$

M is the parameter of pore collapse function. p_{cc} is related to the hydrostatic pore collapse strength p_c.

$$p_{cc} = p_c(\frac{\dot{\varepsilon_{v,pl}}}{\dot{\varepsilon_0}})^b \tag{4.20}$$

$\dot{\varepsilon_0}$ is the reference volumetric plastic strain rate and the exponent b is a material parameter. p_c is a function of plastic volume strain and hardening parameters, thus the yield function can harden with progressing the pore collapse. Moreover, p_c is a time dependent parameter that lead to shrink of the yield function by time. As a result, the chalk volume is declining as a time while stresses are constant. This processes is called creep. The strength and stiffness of chalk is depending on the amount of water present in the rock, which has been mentioned in some studies [59, 64, 29]. By varying the amount of water both elastic young modulus and ultimate strength vary. In the ISAM-GEO chalk model, the pore collapse strength is reduced by increasing the water mass fraction in pore spaces. However, in this work the variation of water saturation is not modeled and the effect of water on weakening the chalk is neglected.

4.3 Damage Model

Irreversible behavior of the fracture such as sliding, which leads to the fracture asperity angle degradation, is modeled by the damage theory. The schematic of a fracture including asperity and aperture is illustrated in Figure 4.1.

Figure 4.1: Fracture with parallel walls, contains asperities

The Fracture opening and the fracture compaction is another types of the irreversible behavior, which are not considered in this work. In order to build a constitutive model for the fracture including the irreversible behaviors, the principal of maximum damage dissipation is employed, and by using the Kuhn-Tucker optimality condition, the damage flow rule is obtained. For more detail about the theory of damage we refer to the work of Ibrahimbegović [36].

The constitutive relation for the fracture can be written as the following form,

$$\Delta\boldsymbol{\varepsilon}'^{d} = \mathsf{F}_{ed}\,\Delta\boldsymbol{\sigma}' \tag{4.21}$$

The elasto-damage compliance tensor F_{ed} can display the irreversible behavior of the fracture. $\Delta\boldsymbol{\varepsilon}'^{d}$ is the total incremental strain of the fracture and similar to the plasticity theory, is sum of the reversible and irreversible strains.

The stress states in fracture model must lie in an admissible region, the boundary between the admissible and the inadmissible region is defined by slip function, which has similarity with the yield function in elasto-plastic materials. The slip function with a negative value corresponds to the reversible behavior of the materials, whereas the zero values indicates the fracture has an irreversible deformation, that indicates the presence of damage. This produces the damage dissipation, which ought to be in agreement with the second thermodynamics principle. By using the principal of the maximum damage dissipation, the damage flow rule to obtain the incremental irreversible damage strain is:

$$\Delta\boldsymbol{\varepsilon}'^{d}_{irr} = \gamma^{d}\frac{\partial\,\boldsymbol{Q}^{d}}{\partial\,\boldsymbol{\sigma}} \tag{4.22}$$

4.3.1 Constitutive model of the Fracture

The constitutive relation of the fracture is defined with respect to the fracture sliding, which is similar to the shear failure in the chalk. The slip F^{d} and potential functions Q^{d} for the single fracture are represented by Mohr-Coloumb function at

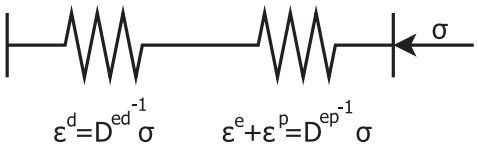

Figure 4.2: Rheological elements: The chalk and the fractured plane are modeled as two springs in series and experience the same applied load.

the local fracture plane coordinates x',y' and z' as follows [40],

$$F^d = \left[\left(\frac{\sigma'_{xy}}{\mu_y}\right)^2 + \left(\frac{\sigma'_{xz}}{\mu_z}\right)^2\right]^{\frac{1}{2}} + \sigma'_{xx} - c_f \tag{4.23}$$

$$Q^d = \left[\left(\frac{\sigma'_{xy}}{\mu_y}\right)^2 + \left(\frac{\sigma'_{xz}}{\mu_z}\right)^2\right]^{\frac{1}{2}} + \sigma'_{xx}\ \sin(\alpha) \tag{4.24}$$

σ'_{xx} is the stress normal to the fracture plane, and σ'_{xy} and σ'_{xz} are shear stresses. c_f is the cohesion of the fracture and μ_y and μ_z are defined as:

$$\mu_y = \tan(\Phi_r + \alpha_y) \tag{4.25}$$

$$\mu_z = \tan(\Phi_r + \alpha_z) \tag{4.26}$$

where Φ_r is the frictional angle and α_y and α_z are the asperity angles of the fractured chalk in the x and z directions. Average asperity angle, α in Equation (4.24) is the average of α_y and α_z [52].

During the deformation of the fracture, degradation of the asperity angle is observed. The asperity degradation is assumed to be a function of the irreversible portion of the fracture displacement.

$$\alpha_y = \alpha_{y0}\ \exp\left(-m|\Delta\varepsilon^d_y|\right) \tag{4.27}$$

$$\alpha_z = \alpha_{z0}\ \exp\left(-m|\Delta\varepsilon^d_z|\right) \tag{4.28}$$

4.4 Coupled Elasto-plastic-damage Model

Neither plasticity nor damage model can present the constitutive behavior of the fractured chalk, for this reason a coupled model is used to consider both damage and plasticity process. For this purpose, the equivalent material is introduced. Gerrard and Pende [22] introduced the rheological scheme for the equivalent material. In this scheme the chalk and the fractured plane are two elements connected in series in form of springs (see Figure 4.2). Series models ensure that each spring experiences

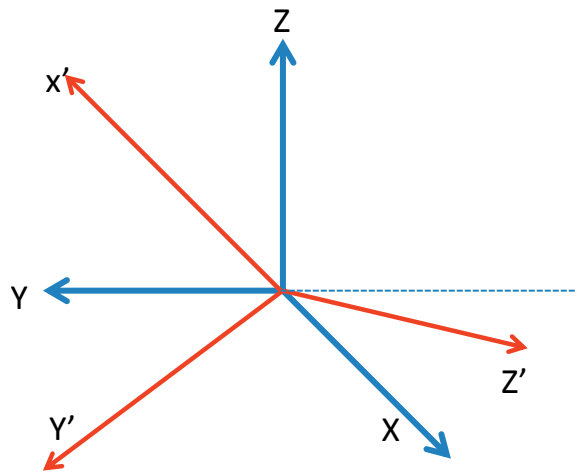

Figure 4.3: Two coordinate axes: the block coordinate, xyz and the fracture coordinate, $x'y'z'$

the same incremental load, and that the total strain is equal to the sum of the strain in each spring, thus the total strain can be split additively into elastic, plastic and damage as,

$$\Delta\varepsilon^t = \Delta\varepsilon^e + \Delta\varepsilon^p + \Delta\varepsilon^d \tag{4.29}$$

In order to introduce an equivalent constitutive model, both fracture and chalk are defined in a same coordinate system.

4.4.1 Coordinate system Transformation

The constitutive of the fracture plane is written in its local coordinate plane (x', y', z'), in order to couple with the chalk, the local coordinate is transferring to the block coordinate (x, y, z) by a transfer matrix, The x' is the axis normal to the fracture plane, The normal direction in the block coordinate is defined by z axis,

$$\begin{Bmatrix} x \\ y \\ z \end{Bmatrix} = \Lambda^T \begin{Bmatrix} x' \\ y' \\ z' \end{Bmatrix} \tag{4.30}$$

$$\Lambda = \begin{Bmatrix} l_x = \cos(x', x) & m_x = \cos(x', y) & n_x = \cos(x', z) \\ l_y = \cos(y', x) & m_y = \cos(y', y) & n_y = \cos(y', z) \\ l_z = \cos(z', x) & m_y = \cos(z', y) & n_y = \cos(z', z) \end{Bmatrix} \tag{4.31}$$

4.4.2 Stress, Strain Transformation

The relationship between stress, strain and constitutive matrix from one coordinate to another coordinate system are explained in the following, more detail are available in Cook et al. [12].

1. Strain Transformation

   Strain transformations are transformations of displacement derivatives. Thus, to relate $\boldsymbol{\varepsilon}'$ to $\boldsymbol{\varepsilon}$, $\frac{\partial u'}{\partial x'}$ is related to $\frac{\partial u}{\partial x}$ with the transform matrix T.

$$\mathsf{T} = \begin{bmatrix} l_x\Lambda & m_x\Lambda & n_x\Lambda \\ l_y\Lambda & m_y\Lambda & n_y\Lambda \\ l_z\Lambda & m_z\Lambda & n_z\Lambda \end{bmatrix} \tag{4.32}$$

$$\boldsymbol{\varepsilon'}^d = \mathsf{T}\boldsymbol{\varepsilon}^d \tag{4.33}$$

2. Stresses Transformation

$$\boldsymbol{\sigma}' = \mathsf{T}^{-T}\boldsymbol{\sigma} \tag{4.34}$$

   where, T^{-T} is defined in the following

$$\mathsf{T}^{-T} = \begin{bmatrix} l_x^2 & m_x^2 & n_x^2 & 2\,l_x\,m_x & 2\,m_x\,n_x & 2\,l_x\,n_x \\ l_y^2 & m_y^2 & n_y^2 & 2\,l_y\,m_y & 2\,m_y\,n_y & 2\,l_y\,n_y \\ l_z^2 & m_z^2 & n_z^2 & 2\,l_z\,m_z & 2\,m_z\,n_z & 2\,l_z\,n_z \\ l_x\,l_y & m_x\,m_y & n_x\,n_y & m_x\,l_y + l_x\,m_y & n_x\,m_y + m_x\,n_y & n_x\,l_y + l_x\,n_y \\ l_y\,l_z & m_y\,m_z & n_y\,n_z & m_y\,l_z + l_y\,m_z & n_y\,m_z + m_y\,n_z & n_y\,l_z + l_y\,n_z \\ l_x\,l_z & m_x\,m_z & n_x\,n_z & m_x\,l_z + l_x\,m_z & n_x\,m_z + m_x\,n_z & n_x\,l_z + l_x\,n_z \end{bmatrix} \tag{4.35}$$

   The rows and columns of the above are arranged in the order xx, yy, zz, xy, yz and xz.

   From Equations (4.33) and (4.34), three elements of strain and stress vectors, which are located in rows of 1, 4 and 6, are taken and used in the constitutive relation of the fracture in its local coordinate system.

3. Constitutive Matrix Transformation

   Stress-strain relationship in the block coordinate is

$$\boldsymbol{\varepsilon\prime}^d = F_J\,\boldsymbol{\sigma\prime} \tag{4.36}$$

$$\mathsf{T}\,\boldsymbol{\varepsilon}^d = F_J\,\mathsf{T}^{-T}\boldsymbol{\sigma} \tag{4.37}$$

   For an orthogonal matrix $\mathsf{T}^T = \mathsf{T}^{-1}$, thus the fracture constitutive matrix at the block coordinate becomes,

$$\boldsymbol{\varepsilon}^d = \mathsf{T}^T\,\mathsf{F}_J\,\mathsf{T}\,\boldsymbol{\sigma} \tag{4.38}$$

4.4.3 Equivalent Linear Elastic Constitutive Model

Since stress in each element is equal to the total stress, the constitutive relationship between strain and stress for the equivalent model with a single fracture is written as follows:

$$\Delta\boldsymbol{\varepsilon}^e = (\mathsf{F}_I + \mathsf{T}^T\,\mathsf{F}_J\,\mathsf{T})\Delta\boldsymbol{\sigma} \tag{4.39}$$

The equivalent compliance matrix of elastic fractured chalk F^t is written as follows:

$$\mathsf{F}^t = \mathsf{F}_I + \mathsf{T}^T\,\mathsf{F}_J\,\mathsf{T} \tag{4.40}$$

4.4.4 Equivalent Elasto-plastic-damage Constitutive Model

Above, the coupled constitutive model for elastic fractured chalk is introduced. However the fractured chalk experience an irreversible deformation that can be explained by coupling the inelastic behavior of damage with the plasticity theory. In this section, a 3-D coupled model that accounts for both inelastic behavior of chalk (plasticity) and fractured (irreversible damage) is introduced. The computational procedure of the coupled model capable of accounting for all inelastic mechanisms is introduced by Ibrahimbegović [36]. The coupled equivalent elasto-plastic-damage constitutive matrix for the fractured chalk is defined according to the series model as follows:

$$D^t = \left[(\mathsf{D}^{ep})^{-1} + (\mathsf{D}^{ed})^{-1}\right]^{-1} \tag{4.41}$$

According to the rheological spring model, both the fracture and the chalk experience the same stress, thus the two following relations are coupled in order to obtain the total strains and damage strains in case with a given applied load.

$$\boldsymbol{\sigma} = \mathsf{D}^t\,\boldsymbol{\varepsilon}^t \tag{4.42}$$

$$\mathsf{D}^{ep}\,(\boldsymbol{\varepsilon}^t - \boldsymbol{\varepsilon}^d) = \mathsf{D}^{ed}\,\boldsymbol{\varepsilon}^d \tag{4.43}$$

4.5 Integration of Nonlinear Constitutive Relations

The constitutive relationship is split into increments. The constitutive relation depends on variables which are depending on the stress-strain state. Since the material behaves nonlinearly, the stress-strain relationship is not constant and the constitutive matrix varies during the loading. As a result, if the incremental step is not small enough, the evaluation of constitutive matrix in each increment lead to large errors. In addition, as mentioned earlier, the stress must lie on or inside the yield surface and slip surface in each increment. If in each increment the yield function becomes greater than zero, it consider as an elasto-plastic condition, if the slip function becomes greater than zero, the damage model is considered and if both the yield and

slip functions are greater than zero the model is the coupled elasti-plastic-damage. Therefor, the initial applied constitutive matrix in the incremental relation was not accurate. A numerical method is used to evaluate the correct elasto-plastic constitutive matrix to ensure the stress state lies on both the yield and slip surfaces. For this reason, the incremental relations must be integrated over an imposed finite loading step. In integration procedure, the incremental constitutive relation is used to obtain the unknown quantity for the finite increment of the known quantity.

4.5.1 Integration Method

Many different integration methods such as Taylor series method and Runge-Kutta methods are available, as well as first order methods such as Euler. The Taylor series expansion is turned into the Euler method if it is truncated to include only first order derivative terms. In this work we use the Euler method to solve the stress-strain relation as describe in the following.

Euler method

The Euler series of a function f at a number of x_0 is

$$f(x_0 + \Delta x) \simeq f(x_0) + \frac{\partial f}{\partial x} \mid_{x_0} \Delta x \tag{4.44}$$

According to the Euler method, if the function is the stress function, the incremental stress defined as:

$$\boldsymbol{\sigma}_1^{tr} = \boldsymbol{\sigma}_0 + \mathsf{F}^{t^{-1}} \Delta \boldsymbol{\varepsilon} \tag{4.45}$$

where $\mathsf{F}^{t^{-1}}$ is the equivalent elastic constitutive matrix obtained from Equation (4.40).

4.5.2 Return Stress Algorithm

To solve the above constitutive equation, the return algorithm proposed by Simo and Ortiz written by Potts and Zdravković [61] is used. In this approach the strains are composed of elastic and plastic and damage strains. These are evaluated independently and then summed. The loading step in Equation(4.45) is assumed to be fully elastic. The trail stress increment are applied to the constitutive model of the chalk and fracture. If the resulting stress increment causes the stress states to lie outside the initial yield surface, the trial stress is corrected by calculating the $\Delta\boldsymbol{\varepsilon}^p$,

$$\boldsymbol{\sigma}_1^{f^p} = \boldsymbol{\sigma}_0^{tr} - \mathsf{D}_I \Delta \boldsymbol{\varepsilon}^p \tag{4.46}$$

The plastic strain are based on the stress conditions from the flow rule,

$$\Delta\varepsilon^p = \gamma^p \frac{\partial \boldsymbol{Q}^p}{\partial \boldsymbol{\sigma}} \tag{4.47}$$

where γ^p is defined in the next section.

If the resulting stress increment causes the stress state to lie outside the initial slip surface, the incremental step is damage.

$$\boldsymbol{\sigma}_1^{f^d} = \boldsymbol{\sigma}_0^{tr} - \mathsf{F}_J^{-1}\Delta\varepsilon^d \tag{4.48}$$

The irreversible damage strain is obtained from the damage flow rule,

$$\Delta\boldsymbol{\varepsilon}_{irr}^d = \gamma^d \frac{\partial \boldsymbol{Q}^d}{\partial \boldsymbol{\sigma}} \tag{4.49}$$

where γ^d is defined in the next section.

The final stresses, which are supplied by the two models should to be equal,

$$\Delta\boldsymbol{\sigma}^f = \boldsymbol{\sigma}^{f^p} - \boldsymbol{\sigma}^{f^d} = 0 \tag{4.50}$$

Thus, an additional iterative procedure is required to enforce the stress equality supplied by two models.

The Plastic and Damage Multiplier

In order to determine the plastic and damage multiplier, the theory of the consistency condition in plasticity and damage theories is applied, which indicates the change in the yield function and the change in the slip function must be equal to zero. By using the chain rule of differentiation, and the Euler expansion method,

$$\Delta F^p(\boldsymbol{\sigma}^p, \boldsymbol{\eta}^p) = \frac{\partial F^p}{\partial \boldsymbol{\sigma}^p}\Delta\boldsymbol{\sigma}^p + \frac{\partial F^p}{\partial \boldsymbol{\eta}^p}\Delta\boldsymbol{\eta}^p \tag{4.51}$$

$$\Delta F^d(\boldsymbol{\sigma}^d, \boldsymbol{\eta}^d) = \frac{\partial F^d}{\partial \boldsymbol{\sigma}^d}\Delta\boldsymbol{\sigma}^d + \frac{\partial F^d}{\partial \boldsymbol{\eta}^d}\Delta\boldsymbol{\eta}^d \tag{4.52}$$

where

$$\Delta\boldsymbol{\sigma}^p = -\mathsf{D}_I\Delta\varepsilon^p = -\mathsf{D}_I\gamma^p\frac{\partial Q^p}{\partial \boldsymbol{\sigma}} \tag{4.53}$$

$$\Delta\boldsymbol{\eta}^p = \gamma^p\frac{\partial Q^p}{\partial \boldsymbol{\varepsilon}} \tag{4.54}$$

and

$$\Delta\boldsymbol{\sigma}^d = -\mathsf{F}_J^{-1}\Delta\varepsilon^d = -\mathsf{F}_J^{-1}\gamma^d\frac{\partial Q^d}{\partial \boldsymbol{\sigma}} \tag{4.55}$$

$$\Delta \boldsymbol{\eta}^d = \gamma^d \frac{\partial Q^d}{\partial \boldsymbol{\varepsilon}} \tag{4.56}$$

By substituting Equation(4.53) and (4.54) into Equation(4.51) and rearranging, the plastic multiplier γ^p can be written as follows,

$$\gamma^p = \frac{\Delta F^p}{\frac{\partial F^p}{\partial \boldsymbol{\sigma}}^T \mathsf{D}_I \frac{\partial Q^p}{\partial \boldsymbol{\sigma}} - \frac{\partial F^p}{\partial \boldsymbol{\eta}^p} \frac{\partial \boldsymbol{\eta}^p}{\partial \boldsymbol{\varepsilon}^p}} \tag{4.57}$$

By substituting Equation(4.55) and (4.56) into Equation(4.52) and rearranging, the damage multiplier γ^d becomes,

$$\gamma^d = \frac{\Delta F^d}{\frac{\partial F^d}{\partial \boldsymbol{\sigma}}^T \mathsf{F}_J^{-1} \frac{\partial Q^d}{\partial \boldsymbol{\sigma}} - \frac{\partial F^d}{\partial \boldsymbol{\eta}^d} \frac{\partial \boldsymbol{\eta}^d}{\partial \boldsymbol{\varepsilon}^d}} \tag{4.58}$$

Plastic and damage multipliers can be evaluated from two different algorithms: explicit and implicit. The explicit method evaluates the variables from the initial conditions. The implicit method evaluates the variables for the final conditions at the end of the loading interval. In this work an explicit method is used, in which the values of the variables are known and obtained from the initial stress states. However, this method may diverge for highly nonlinear functions.

Correction of the Initial Stresses

Because the stress and other variable are determined by first order integration (Euler method), the final stress points can be estimated with considerable truncated errors. Consequently the plastic multiplier at this stress states may be evaluated with errors; although the consistency equation is satisfied, the stress states may lie outside the yield surface. Thus, an iterative procedure is required to determine the final stress point and final yield surface and to ensure that the constitutive relation is satisfying the yield and slip criterion. Figure 4.4 illustrate the stress correction by the explicit return algorithm

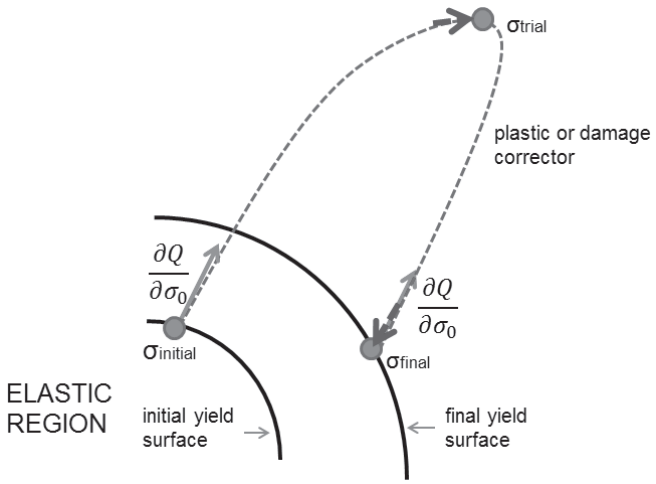

Figure 4.4
Explicit procedure of the stress correction by the return algorithm

Chapter 5

Coupled Fluid Flow with Constitutive Model

As mentioned, chalk is a porous media and pores are filled with fluid. Pore pressure is incorporated to the constitute equation in such a way that the total stress is divided into effective stress,$\boldsymbol{\sigma}^{t\prime}$, which are acting in the rock structure, and the pore pressure p. The effective stresses defined in Equation (5.1), are used in the constitutive relation.

$$\boldsymbol{\sigma}^{t\prime} = \boldsymbol{\sigma} - \alpha_{\text{Biot}}\, p \tag{5.1}$$

where α_{Biot} is called Biot's coefficient. This coefficient represents the ratio of the volume of water squeezed out of the rock to the total volume change for deformation at constant fluid pressure. In this work the value of α_{Biot} equals one, which indicates that the grains compressibility are insignificant.

The coupling between the flow model and the stress states of the solid structure has been done by a one way coupling; The flow field is a function of position from the previous increment. At each time step the flow field can be solved independently of the stress field, and the pressure gradients are solved. The stress states can be evaluated once the flow field has been determined. The known pressure gradients contributes to the force, and used in the constitute model to calculate the stress states.

Chapter 6

Numerical analysis

The computational method of the fluid flow is based on the Finite Volume method, whereas the Finite Element method is used to evaluate the stress states of the rock.

6.1 Finite volume

The continuity and transport equations are solved by finite volume method available in the in-house software "Brilliant". Finite volume methods are described in [19], and their description is omitted here.

From integrating the continuity and Darcy equations over the finite control volume, the pressure at the center of each control volume is evaluated. The pressure differences between centers of two neighboring control volumes is used to determine the pressure gradients. Pressure gradients acts as forces on the common surface between two control volume (see Figure 6.1). The nodal forces of each element can be interpolated from the pressure gradient on the surface and by using a shape function within a finite element.

$$\Delta \boldsymbol{f} = \int_V \mathsf{B}^T \Delta P dV \tag{6.1}$$

6.2 Finite Element

The finite element formulation is explained in detail in several references such as [12, 61]. In this work, the nonlinear Finite element code used to analyze the fractured chalk structure is implemented in an in-house C++ software "Brilliant". The elements are 3-D hexahedron elements with 8 nodes and 8 integration points referred to as Gauss points. Strain and stress vectors are evaluated at the integration

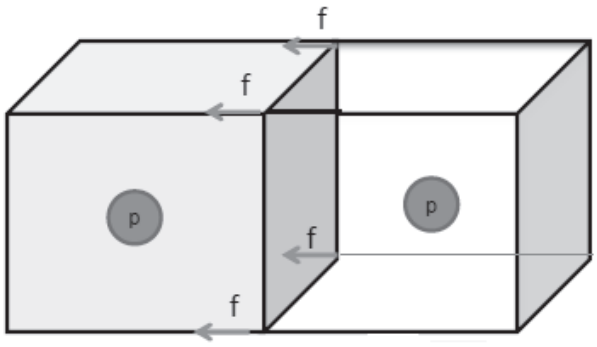

Figure 6.1: Two neighboring control volumes: pressure p is stored at their center and forces f are applied on the common nodes

points, while vectors of displacement and forces are defined at the nodes of each element. The detailed description of the finite element method is omitted here.

The method to find the initial stresses from the given displacements or loads is explained in the following. For the structure being analyzed, the vector of incremental nodal displacement is related to the vector of applied incremental nodal forces by the global stiffness matrix K_g:

$$\Delta \boldsymbol{f} = \mathsf{K}_g \Delta \boldsymbol{u} \tag{6.2}$$

The global stiffness matrix,K_g, is calculated from sum up of all elements stiffness matrices:

$$\mathsf{K}_g = \int_V \mathsf{B}^T \mathsf{D}^t \mathsf{B} dV = \sum_{e=1}^{n} \int_{V_e} \mathsf{B}_e^T \mathsf{D}^t \mathsf{B}_e dV \tag{6.3}$$

where D^t is the coupled elasto-plastic-damage constitutive matrix at the current Gauss point. If the material is considered as an elaso-plastic without any damage (intact chalk without the fractures), the constitutive matrix is replaced by D_{ep}.

V is the element volume and B is representing the derivatives of the element shape function giving the strain-displacement relationship [30].

$$\Delta \boldsymbol{\varepsilon} = \mathsf{B} \Delta \boldsymbol{u} \tag{6.4}$$

The incremental trial stress is assumed to be elastic and defined from the following equation.

$$\boldsymbol{\sigma}^{tr} = \boldsymbol{\sigma}^0 + \Delta \boldsymbol{\sigma}^e = \boldsymbol{\sigma}^0 + \mathsf{D}_e^t \Delta \boldsymbol{\varepsilon} \tag{6.5}$$

where D_e^t is the equivalent elastic constitutive matrix.

The stress correction between trail and final stress is converted into a nodal element force vector:

$$\Delta \boldsymbol{f}^{el} = \int_{V_e} \mathsf{B}_e^T \Delta \boldsymbol{\sigma} dV \tag{6.6}$$

where $\Delta \boldsymbol{\sigma}$ is the difference between the trial stress vector and the final stress vector, which is obtained by the Return algorithm and lies on both the yield and the slip surfaces.

$$\Delta \boldsymbol{\sigma} = \boldsymbol{\sigma}^t - \boldsymbol{\sigma}^f \tag{6.7}$$

$\Delta \boldsymbol{f}^{el}$ is added to in Equation (6.3) to calculate the displacement vectors and later strains and stresses vectors. This algorithm is iterating until $\Delta \boldsymbol{f}^{el}$ balances the applied forces; it indicates that applied external forces on the structure are equal to the sum of all elements internal forces and the structure is on global force equilibrium.

Chapter 7

Summary of the papers

7.1 Paper 1

Analysis of Failure in Fractured Chalk by Implementing a Coupled Elasto-plastic-anisotropic Damage Constitutive Model in Finite Element Model

In this paper, a coupled elasto-plastic-damage constitutive model for the fractured chalk is developed and implemented in the in-house Finite Element code. The influence of the fracture orientation on the chalk strength and the overall deformation is investigated.

7.2 Paper 2

Coupled Fluid Flow and Elasto-plastic Damage Analysis for Fractured Porous Chalk with Induced Wormhole

In this paper, the fractured chalk including an induced wormhole is modeled. The geomechanical model including the elasto-plastic-damage constitutive model is coupled with the flow model in porous media. An anisotropic permeability tensor due to the existence of the natural fractures is introduced. The strength and deformation of the chalk and wormhole are analyzed during production flow and effects of the fracture orientation with respect to the wormhole on both the flow and the chalk strength are studied.

7.3 Paper 3

Effects of the Natural Fracture Orientations on the Porosity Evolution and Stress Distribution during the Dissolution of a Porous Media: Computational Simulation with Coupled Flow and Elastic Fractured Rock

In this paper, the dissolution of the chalk due to the acid injection is modeled by including the transport and porosity evolution equations to the previous models. Different dissolution patterns as a result of the different fracture orientation cause different porosity filed in the chalk, which then influence the stress states of the chalk.

Chapter 8

Conclusion

Presence of the pre-exsiting fractures in the chalk such as natural fractures and created fractures during the previous acid treatments or hydraulic fracturing influence the overall deformation and stress states of the chalk. Chalk tends to deform along the fracture plane, thus in the uniaxial simulation, high deviatoric stresses are localized along the fracture, which facilitate the chalk failure. Results from the computational simulations demonstrate that the plastic deformation along the fracture increases if the fracture dip angle increases. For example, in cases include fracture planes with dip angles of 20° and higher, a high plastic deformation is captured.

Fractures change the permeability of the rock and creates paths of less resistance for the flow along the fractures. If the fractures and wormhole are located along the well, production can improve. However, the direction of the wormhole and fractures in respect to other fractures affect the recovery. Presence of horizontal fractures increase the chalk vertical deformation under compression load and occlude the horizontal wormhole and neutralize its effect on the recovery. On the other hand, inclined fractures from the horizon increase the risk of the shear failure and damage around the wormhole.

Permeability changes due to existence of fractures influence the heterogeneity of the media and affect the further acid treatment by creating a favorable flow path for the acid, therefore it leads to a specific dissolution pattern and porosity field in the chalk. The fracture plane orientated parallel to the plane between the well and reservoir has the best penetration depth through the chalk core sample, therefore it can improve the fluid production: for example a core sample includes a fracture plane with a dip of 90° and azimuth 90° and acid is injecting from the inlet on top of the core.

Chapter 9

Recommendations for Future Studies

It has been shown that the chalk porosity is evolving during the acid injection and the rock heterogeneity is one factor that affect the porosity profile. As mentioned, the chalk may fail due to the pore collapse. The pore collapse strength of the chalk depends on the porosity parameters. Therefore, porosity development during the acid injection leads to changes of the pore collapse strength and increase the risk of the rock failure due to the pore collapse. For the future study, the parameter of pore collapse yield function during the porosity development can be updated and the risk of the pore collapse for different dissolution patterns investigated. Moreover, the model can be improved by implementing several natural or pre-existing fractures with random orientations. In addition, the detailed model of the reaction of acid with the rock can be included in this model in order to relate the created dissolution patterns to the acid parameters.

Appendix A

Appendix A

Analysis of Failure in Fractured Chalk by Implementing a Coupled Elasto-plastic-anisotropic Damage Constitutive Model in Finite Element Model

By Nazanin Jahani, Bjørn Haugen and Geir Berge; submitted to *Computers and Geotechnics*.

Abstract

Rock is a natural geological material with discontinuities. Discontinuities include natural fractures and fractures created by chemical reactions as well as hydraulic fracturing. These discontinuities weaken the rock and have significant effects on the deformations and strength of the rock. A numerical constitutive model can give understanding of the physical behavior of the rock and is an effective tool to describe the behavior of the fractured rock for large models.

In this work a computational continuum model is developed and implemented in a multi-physics finite element code. The model is able to predict the elastic and inelastic deformations of rock and fractures simultaneously. The model accounts for plasticity in combination with damage for the fracture. The coupled elastic-plastic-damage constitutive model for the fractured rock is introduced based on

decomposition of deformation in both intact rock and fracture. The rock material in this work is a porous chalk. The intact chalk is assumed to be isotropic whereas the fracture has an anisotropic constitutive model.

Numerical results show that the fracture and its orientation influences the deformation of the chalk both for elastic and plastic deformation, and that fractured chalk is weaker compared to its corresponding intact chalk. Strength of the chalk depends on the fracture dip angle and the fracture orientation.

A.1 Introduction

Rock is a natural geological material; anisotropic, inhomogeneous, inelastic and naturally fractured. The physical behavior of rock under different distributed stress states is complex. Using a computational model is an effective way to capture the rock's physical behavior and enhance understanding of the processes involved by studying the effect of changing boundary conditions and input parameters on output results. Different numerical methods have been developed for rock mechanics problems for different purposes. The most commonly applied numerical methods can be classified as continuum and discontinous methods. Several good review papers, such as Jing and Hudson [39], Jing [38], presents current techniques in numerical modeling and their application in rock mechanics. Discontinous methods are mostly used in cases with large deformations or complete detachments, such as a fracture opening during hydraulic fracturing in oil reservoirs. In contrast, continuum methods are applied when materials are not broken apart, such as naturally fractured rock mass.

The most commonly used continuum based computational method for fractured rock masses is the Finite Element Method (FEM). In this method, the discontinuity is introduced by a joint or fractured plane in the rock material, and an equivalent constitutive matrix is implemented in the FEM code. In the approaches presented in the available literature [52, 40, 2, 66, 67, 56, 10, 22], the sliding of the fracture plane is modeled by anisotropic damage in a way similar to classic plasticity theory, and intact rock is assumed to be elastic. However, chalk has significant plastic deformation in cases of shear failure or pore collapse: a model is therefore needed to couple plasticity and damage.

Several authors [41, 65, 9] used an equivalent constitutive model in the finite element (FE) code that couples the elasto-plastic deformation of rock with the deformation of the fracture plane; fracture deformation is modeled by damage theory. This has been done using the scalar damage parameter introduced by Kachanov [42]. Their model of damage maintains isotropy, and all stress components are modified equally. However, in reality, the fracture plane deforms very differently in the normal and shear directions.

In the work of Rafeh et al. [63], fractured chalk is modeled by proposing an anisotropic constitutive damage formulation in analogy to plasticity [7, 8]. In this model, failure of intact rock is decoupled from the damage model: the calculated stress from the plasticity model is applied to each fractured plane, which results in underestimation of the deformation of the fractured plane.

In our model, fractured chalk is modeled by introducing an equivalent coupled elasto-plastic-damage constitutive model considering anisotropic damage. It is assumed that each fracture plane experiences the same stress as the rock material. The model shows that the presence of fractures increase the deformation of the chalk and accelerates shear failure.

A.2 Methods

The coupled elasto-plastic and damage model that we employ is based on the model presented by Ibrahimbegović et al. [35]. Damage and plasticity constitutive models and their coupling are defined based on three hypotheses:

1. Linear decomposition of the total strain into elastic, plastic and damage strains.
2. Strain stored in a body due to the deformation as sum of the elastic, plastic and damage parts
3. Yield criteria and flow rules for both plasticity and damage

The parameters for the yield function for the plasticity model were provided by ISAMGEO GmbH [60] (see A.B). The parameters for the slip function for damage, which delimits reversible damage deformation, are as reported by Jing et al. [40].

A.2.1 Elasto-plastic-damage Modeling of Chalk with Fractured Plane

Deformation of intact chalk is modeled by an elasto-plastic constitutive model. Discontinuous fracturing phenomena are then presented by introducing the continuum model for damage, and at the end, a coupled elasto-plastic-damage constitutive model is presented to demonstrate deformation of the fractured chalk.

Deformation of intact chalk is composed by elastic and plastic deformation. The elasto-plastic constitutive relation for intact chalk consists of the elastic and elasto-plastic models described in the following sections.

Elastic Model

The constitutive relation for the linear elastic material is:

$$\Delta\boldsymbol{\sigma} = \mathsf{D}_I \Delta\boldsymbol{\varepsilon}^e \tag{A.1}$$

D_I is the constitutive matrix as defined in A.A, and $\Delta\boldsymbol{\varepsilon}^e$ is the incremental elastic strain.

Plastic Model for Intact Chalk

Chalk fails due to high shear stresses defined by the modified Mohr-Coulomb yield surface F^p and the potential function Q^p, and due to pore collapse. The yield surfaces for shear failure are expressed in terms of stress invariant through the modified Mohr-Coulomb yield surface F^p and potential Q^p as:

$$F^p = \sqrt{J_2}\left\{\cos(\theta) - \frac{\sin(\phi)\,\sin(\theta)}{\sqrt{3}} - \zeta\,\left[2\cos(2\theta) - 1\right]\right\} + \\ - \left[p_m\,\sin(\phi) + c\,\cos(\phi_{\text{peak}})\right] \quad \text{(A.2)}$$

$$Q^p = \sqrt{J_2}\left\{\cos(\theta) - \frac{\sin(\psi)\,\sin(\theta)}{\sqrt{3}} - \zeta\,\left[2\cos(2\theta) - 1\right]\right\} + \\ - \left[p_m\,\sin(\psi) + c\,\cos(\psi_{\text{peak}})\right] \quad \text{(A.3)}$$

where J_2 is the second invariant of deviatoric stress, p_m is the mean stress (one third of the first stress invariant; the trace of the stress tensor), θ is the Lode's angle and ζ scales the impact of the intermediate principal stress. ϕ is the friction angle and c is the cohesion, which are both varying due to hardening and softening. Note that the plastic potential Q^p is described by the same function as the yield. However, the friction angle ϕ is replaced by the dilatancy angle ψ. In order to have a realistic description of the volumetric plastic strain changes, a non-associated flow rule is used.

Hardening of the yield surface is applied to the model by increasing the friction angle before shear strength reaches the peak stress. After reaching the peak stress, the material experiences pronounced softening by decreasing cohesion and friction angle. For the dilatancy angle ψ, the hardening and softening are the same as for the friction angle ϕ. The incremental plastic strain $\Delta\boldsymbol{\varepsilon}^p$ and the elasto-plastic constitutive matrix D^{ep}, are defined with a plastic flow rule and implementing an iterative algorithm in the FE code. The iterative algorithm proposed by Ortiz and Simo [54] brings the stress state back towards the yield surface until the yield function is satisfied.

The yield surface for pore collapse is defined by an ellipse in the $J_2 - p_m$ space, and it is assumed that the shear failure has priority over pore collapse. The model is developed by Plischke [60].

A.2.2 Anisotropic Damage Model for Fractured Chalk

Deformation of fractures is modeled by damage theory. The damage model used in this work was introduced by Ortiz and Simo [54] and further explained by Ibrahimbegović [36]. In this approach, the fracture plane's constitutive relation is formulated in the framework developed for the elasto-plastic chalk material with the following assumptions:

1. The fractured surface is planar.
2. The orientation of the fracture is fixed during the entire computational process.
3. The elastic constitutive matrix for fractures is anisotropic.

The normal displacement of the fracture is represented by tension or crack opening, while compressive deformation is represented by frictional sliding or shear deformation. In this work only the sliding displacement or shearing of the fracture plane is implemented.

Elastic Constitutive Equation of a Single Fracture

From the second principle of thermodynamics and the principle of maximum damage dissipation, which for an elastic process is equal to zero, the elastic compliance matrix of the single fracture in the local coordinate takes the following form:

$$\Delta\boldsymbol{\varepsilon}^d = \mathsf{F}_J \Delta\boldsymbol{\sigma} \tag{A.4}$$

where $\Delta\boldsymbol{\sigma}$ is the stress incremental of the fracture and $\Delta\boldsymbol{\varepsilon}^d$ is the strain incremental vector of the fracture or damage strain and F_J is the compliance matrix of the fracture plane written as below:

$$\mathsf{F}_J = \begin{bmatrix} k_n^{-1} & 0 & 0 \\ 0 & k_s^{-1} & 0 \\ 0 & 0 & k_t^{-1} \end{bmatrix} \tag{A.5}$$

where k_n is the stiffness normal to the fracture plane, and k_s and k_t are the shear stiffness of the fracture plane in two orthogonal directions in the local coordinates of the fracture plane [52].

Irreversible Deformation of the Fracture Plane

Frictional sliding in the fracture is an irreversible deformation, which is represented by irreversible damage in a way similar to developing plasticity in chalk material

[36]. Jing et al. [40] proposed yield and potential functions for a single fracture as shown below:

$$F^d = \left[\left(\frac{\sigma'_{xy}}{\mu_x}\right)^2 + \left(\frac{\sigma'_{xz}}{\mu_z}\right)^2\right]^{\frac{1}{2}} + \sigma'_{xx} - c_f \tag{A.6}$$

$$Q^d = \left[\left(\frac{\sigma'_{xy}}{\mu_x}\right)^2 + \left(\frac{\sigma'_{xz}}{\mu_z}\right)^2\right]^{\frac{1}{2}} + \sigma'_{xx}\ \sin(\alpha) \tag{A.7}$$

where c_f is the cohesion of the fracture and μ_x and μ_z are defined as:

$$\mu_x = \tan(\Phi_r + \alpha_x) \tag{A.8}$$

$$\mu_z = \tan(\Phi_r + \alpha_z) \tag{A.9}$$

where Φ_r is the frictional angle and α_x and α_z are the asperity angles of the fractured chalk in the x and z directions. Average asperity angle, α in equation A.7 is the average of α_x and α_z [52].

During the deformation of the fracture, degradation of the asperity angle is observed. The asperity degradation is assumed to be a function of the irreversible portion of the fracture displacement.

$$\alpha_x = \alpha_{x0}\ \exp\left(-m|\varepsilon_x^d|\right) \tag{A.10}$$

$$\alpha_z = \alpha_{z0}\ \exp\left(-m|\varepsilon_z^d|\right) \tag{A.11}$$

The elastic-irreversible damage constitutive equation represents the deformation of a fracture in analogy to the plasticity model of the intact chalk. The damage constitutive matrix is D^{ed} and the incremental damage deformation is $\Delta\boldsymbol{\varepsilon}^d$. See A.B.

A.2.3 The Equivalent Coupled Elasto-Plastic-Damage Constitutive Model for the Fractured Chalk

In order to analyze the deformation of the fractured chalk, neither the plastic nor the damage theory are sufficient to describe the physical behavior of the material: therefore, an equivalent constitutive model is needed to describe both processes. In this model, a coupled constitutive model is introduced, assuming that each fracture plane experiences the same stress as the chalk, and that the total strain is the sum of the strains in fracture and chalk. The coupled constitutive model is divided into two parts: an elastic-damage model and an elasto-plastic irreversible damage model, as explained in the following sections.

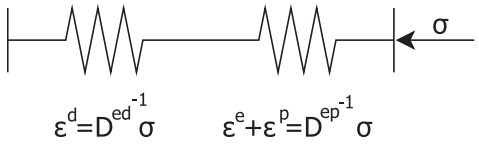

Figure A.1: Rheological elements: chalk and the fractured plane are modeled as two springs in series and experience the same applied load.

Equivalent Elastic Constitutive Model

Gerrard and Pende [22] introduced the rheological scheme of Figure A.1 for the equivalent material. In this scheme chalk and the fractured plane are two elements connected in series in form of springs. Series models ensure that each spring experiences the same incremental load, and that the total strain is equal to the sum of the strain in each spring:

$$\Delta\varepsilon^t = \Delta\varepsilon^e + \Delta\varepsilon^p + \Delta\varepsilon^d \tag{A.12}$$

Since stress in each element is equal to the total stress, the constitutive relationship between strain and stress for the equivalent model with a single fracture is written as follows:

$$\Delta\varepsilon^t = (\mathsf{F}_I + \mathsf{T}^T \mathsf{F}_J \mathsf{T})\Delta\boldsymbol{\sigma}^t \tag{A.13}$$

where F_I is the elastic compliance matrix of the chalk without fracture and F_J is the compliance matrix of elastic fracture plane in its local coordinates. The equivalent compliance matrix of elastic fractured chalk F^t is written as follows:

$$\mathsf{F}^t = \mathsf{F}_I + \mathsf{T}^T \mathsf{F}_J \mathsf{T} \tag{A.14}$$

T is a 6×3 transformation matrix [10**?**] (defined in A.C) that transforms the stress vector of each block into the stress vector at the local coordinates of the fracture plane as follows:

$$\begin{Bmatrix}\sigma'_{xx} & \sigma'_{xy} & \sigma'_{xz}\end{Bmatrix}^T = \mathsf{T}\begin{Bmatrix}\sigma_{xx} & \sigma_{yy} & \sigma_{zz} & \sigma_{xy} & \sigma_{yz} & \sigma_{xz}\end{Bmatrix}^T \tag{A.15}$$

the corresponding strain coordinate transformation is:

$$\mathsf{T}^T\begin{Bmatrix}\varepsilon'_{xx} & \varepsilon'_{xy} & \varepsilon'_{xz}\end{Bmatrix}^T = \begin{Bmatrix}\varepsilon_{xx} & \varepsilon_{yy} & \varepsilon_{zz} & \varepsilon_{xy} & \varepsilon_{yz} & \varepsilon_{xz}\end{Bmatrix}^T \tag{A.16}$$

where the strain vector on the right-hand side is the deformation of the fracture plane.

Equivalent Elasto-plastic-damage Constitutive Model

Above, the coupled constitutive model for elastic fractured chalk is introduced. However the fractured chalk experience an irreversible deformation that can be explained by coupling the inelastic behavior of damage with the plasticity theory. In this section, a 3-D coupled model that accounts for both inelastic behavior of chalk (plasticity) and fractured(irreversible damage)is introduced. The computational procedure of the coupled model capable of accounting for all inelastic mechanisms is introduced by Ibrahimbegović [36]. The coupled equivalent elasto-plastic-damage constitutive matrix for the fractured chalk is defined according to the series model (Figure A.1) as follows:

$$D^t = \left[(\mathsf{D}^{ep})^{-1} + (\mathsf{D}^{ed})^{-1} \right]^{-1} \tag{A.17}$$

When both plasticity and irreversible damage are active, each model modifies stress component in two separate computations and independent of each other. We must make sure that the final stress values produced by the two stress return algorithms produce the same stress to satisfy our rheological spring model. The return algorithm described by Ortiz and Simo [54] is used to modify stresses and return them back on to the yield and slip surfaces. At the end of each computation, stresses provided by the two models will be enforced to be equal by using an additional iterative loop. The computational procedure used to find the stress state of the fractured chalk using the coupled model is :

1. Calculate the equivalent constitutive matrix D^t and assemble the global system constitutive matrix K .

   At the beginning of the solution an elastic constitutive matrix is used.

2. Solve $\mathsf{K}\,\Delta\mathbf{u} = \Delta\mathbf{F}$ by the FEM to find the first estimate of nodal displacements. $\Delta\mathbf{u}$ is the vector of incremental nodal displacements and $\Delta\mathbf{F}$ is the vector of nodal incremental loads.

3. Calculate the incremental elastic nodal strains for each integration node, $\Delta\boldsymbol{\varepsilon}$

4. Obtain the trial stress at time m:

   $$\boldsymbol{\sigma}_n^{k^m} = \boldsymbol{\sigma}^{m-1} + \mathsf{D}_n^t \Delta\boldsymbol{\varepsilon}_n^t \tag{A.18}$$

   where m is the current time m. n is the number of iteration in the return algorithm at the current time m. k is the number of iteration through the coupling of the plastic and damage algorithm. According to the rheological spring model, stresses are equal at each element(spring) and strains of elements(springs) are additive. Stresses at each time step formulated as:

   $$\boldsymbol{\sigma}_n^k = \mathsf{D}_n^t\,\boldsymbol{\varepsilon}_n^t = \mathsf{D}_n^{ep}\,(\boldsymbol{\varepsilon}_n^t - \boldsymbol{\varepsilon}_n^d) = \mathsf{D}_n^{ed}\,\boldsymbol{\varepsilon}_n^d \tag{A.19}$$

5. Obtain the irreversible deformations and update the stress vector and the constitutive matrix by using the coupled elasto-plastic-damage computational procedure as it is displayed in Table A.1.

   The procedure in Table A.1 is an iterative algorithm until equal stresses are produced by the damage and plastic sub-algorithms.

6. Repeat the procedure until the internal forces are equal to the external forces.

A.2.4 Input parameters and geometry

In this section the proposed 3-D model is applied to a chalk core plug under uni-axial compression load. The choice of chalk strength parameters and fracture parameters is listed in Table A.2.

A.3 Numerical Results and Discussion

The numerical results are obtained with an in-house FEM code [5] presented in this section. First the presented model is analytically verified and then results for the elasto-plastic-damage model for the fractured chalk under uni-axial compression load are demonstrated.

A.3.1 Model Verification

In this section the 3-D finite element code for the elastic fractured chalk is verified. In the elastic part, the overall compliance matrix is constant.

Elastic Deformation

Since the constitutive matrix is constant, in the elastic part a single time step is sufficient to find deformations. The test case presented here is rectangular volume $1\,\text{m} \times 1\,\text{m} \times 2\,\text{m}$, see Figure A.2. Three faces of the cube (the bottom face and two horizontal faces in x and y directions) have zero displacements in their normal directions , the rest of three faces are free to move. 1 MPa pressure load applied to the upper surface. The fracture is on the horizontal plane intersect the intact rock. Young modulus E of intact rock is 100 GPa and the normal fracture stiffness, K_n, is $20\,\text{GPa}/\text{m}$.

Vertical displacements are calculated from:

$$\boldsymbol{\varepsilon} = \mathsf{F}^t \boldsymbol{\sigma} \tag{A.20}$$

Table A.1: Computational procedure for obtaining the constitutive model of the anisotropic coupled-plasticity-damage model

<table>
<tr><td colspan="2">Take the trial stress, $\boldsymbol{\sigma}_n^k$, from equation (A.18)</td></tr>
<tr><td colspan="2">Find stresses and strains on the fracture plane coordinates by using the matrix transformations $\boldsymbol{\varepsilon}_n^d = \mathsf{T}^T\,\mathsf{F}_J\,\mathsf{T}\,\boldsymbol{\sigma}_n^k$ and $\boldsymbol{\sigma}_n'^k = \mathsf{T}\,\boldsymbol{\sigma}_n^k$</td></tr>
<tr><td>Plasticity model
1. Give the trial stress, $\boldsymbol{\sigma}_n^k$, to the plasticity model.
2. Check the yield surface of the plasticity model, using the iterative return algorithm until stresses return back onto the yield surface.
3. Calculate the plastic deformation.
4. Update the elasto-plastic constitutive matrix, D_{n+1}^{ep}.
5. Update the stress vectors, $\boldsymbol{\sigma}_{n+1}^k$.</td><td>Damage model
1. Give the trial stress on fracture coordinates, $\boldsymbol{\sigma}_n'^k$, to the damage model.
2. Check the slip surface of the damage model, using the iterative return algorithm until stresses return back onto the slip surface.
3. Calculate the irreversible deformation.
4. Update the damage constitutive matrix, D_{n+1}^{ed}.
5. Update stress vectors on fractured plane coordinates, $\boldsymbol{\sigma}_{n+1}'^k$.
6. Calculate damage strain on fractured plane coordinates, $\boldsymbol{\varepsilon}'_{n+1} = \mathsf{F}_J\,\boldsymbol{\sigma}'_{n+1}$
7. Update the given damage strain in the block coordinates, $\boldsymbol{\varepsilon}_{n+1}^d = \mathsf{T}^T\,\boldsymbol{\varepsilon}'$.
8. Calculate the difference of the damage strain in the block coordinates $\Delta\boldsymbol{\varepsilon}_{n+1}^d = \boldsymbol{\varepsilon}_n^d - \boldsymbol{\varepsilon}_{n+1}^d$.</td></tr>
<tr><td colspan="2">Note: If the $\Delta\boldsymbol{\varepsilon}_{n+1}^d = 0$ the stress produced by plasticity and damage model are equal and the calculation continues to the next time step $(m+1)$, otherwise:</td></tr>
<tr><td colspan="2">Update the given trial stresses, $\boldsymbol{\sigma}_{n+1}^{k+1} = \mathsf{D}_{n+1}^{ep}\,(\boldsymbol{\varepsilon}_{n+1}^t - \boldsymbol{\varepsilon}_{n+1}^d) = \boldsymbol{\sigma}_{n+1}^k + \mathsf{D}_{n+1}^{ep}\,\Delta\boldsymbol{\varepsilon}_{n+1}^d$</td></tr>
<tr><td colspan="2">Repeat the calculation from the beginning of this table</td></tr>
</table>

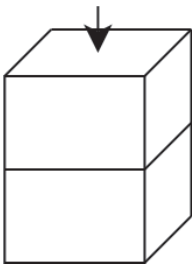

Figure A.2: The sketch of the single horizontal fracture plane

Table A.2: Chalk and fracture parameters assumed for analyses

Young's modulus, E	4000 MPa
Poisson's ratio, ν	0.22
Angle of friction for yield (initial, peak, residual), Φ	37.5°, 38°, 37.7°
Angle of friction for potential surface, Ψ	19°
Cohesion (initial, peak, residual), c	0.8 MPa, 0.8 MPa, 0.7 MPa
Fracture normal strength, k_n	30 MPa/m
Fracture shear strength, k_s, k_t	15 MPa/m, 15 MPa/m
Fracture cohesion, c_f	0
Fracture asperity angle (initial), α_x, α_z	10°, 10°
Fracture angle of friction, Φ_r	37.5°

In this model, only one normal element of stress, σ_{zz}, is non-zero, then only the third column of the total compliance matrix is needed to calculate strains, and vertical displacements are calculated from:

$$\Delta U_z = \sigma_{zz} \left(\frac{1}{k_n} + \frac{1}{E} \right) H \tag{A.21}$$

where H is the volume height. The numerical results and analytical give us a vertical displacement of 6 mm.

The fracture plane orientation is defined by the dip and strike angles (See A.C for definition of the dip and strike angles) . When the fracture plane has an angle with the horizontal plane(xy plane), which means a dip angle greater than zero, the applied normal stress induces shear stresses as a results of the non-symmetric and anisotropic constitutive matrix, which represents the anisotropic nature of the fractured chalk. In the following, the computational results of the coupled elasto-plastic-damage model including a fracture plane with different orientations are presented.

A.3.2 Numerical Simulation of the Coupled Elasto-plastic-damage model

In this section, the FEM results of the coupled elasto-plastic-damage model for a chalk plug with induced fractured plane are presented.

The model geometry consists of a rectangular volume of 2 m in vertical direction, z, and 1 m in horizontal, x and y directions. The simulation has been done for the chalk includes a single fracture with different dip angles increasing from 0° to 90°.

Displacement for faces normal to x and y directions are zero in their normal directions. The bottom surface has zero displacement in z direction, and vertical compression load is applied on the top surface. Boundary load is changed from 0 MPa to 11 MPa in 80 seconds.

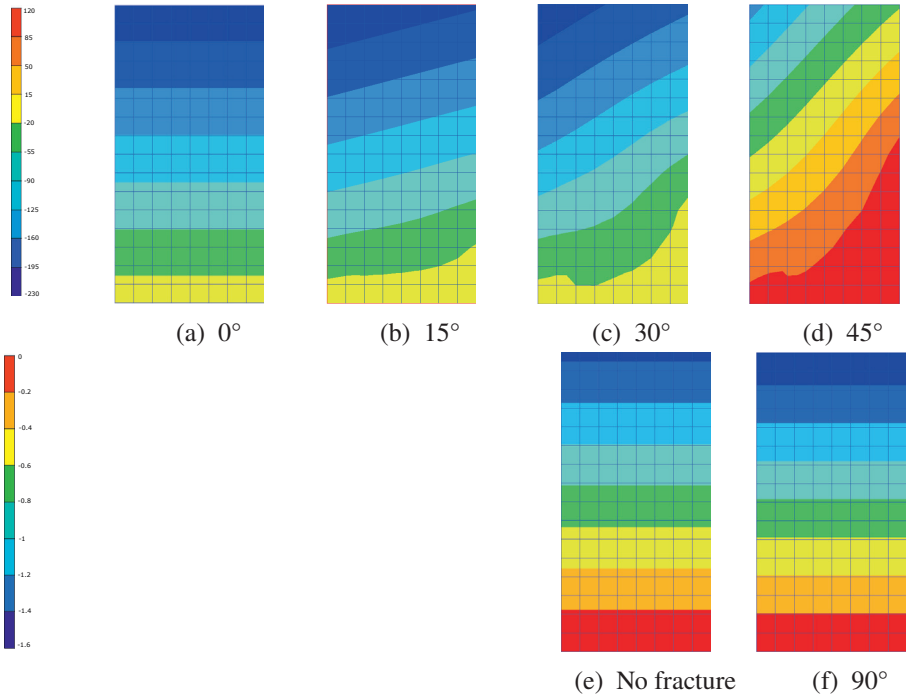

(a) 0° (b) 15° (c) 30° (d) 45°

(e) No fracture (f) 90°

Figure A.3: Vertical displacements $[mm]$ in the middle of the loading (time 25 seconds) for the intact chalk (Fig. A.3e) and the fractured chalk with different dip angles (Fig. A.3a, A.3b, A.3c, A.3d, A.3f) : chalk deforms along the fracture

The results demonstrate the presence of the fracture in the chalk and its orientation has a strong effect on the stress distribution and deformation of the chalk sample. In Figure A.3, vertical deformation of the fractured chalk with different dip angles are compared and compared with the intact chalk. The horizontal fracture (dip angle=0°) shows the highest vertical displacement, while the chalk with the vertical fracture plane (dip angle = 90°) deforms as the same as the intact chalk. From Figure A.3 can be seen the chalk tends to deform along the fracture plane.

The fractured plane induces anisotropy and increases the non-symmetric nature of the constitutive matrix, which induces higher shear stresses. Shear stresses change with the change of the fracture orientation. Higher shear stresses facilitate the shear failure of the chalk. In this work, fracture plane with dip angles of 0°, 15°, 30°, 45° and 90° are compared. Results shows that at dip angles 30° and 45°, the shear stresses are significant and chalk experiences a higher and an earlier plastic deformation in compare with the intact chalk. In Figure A.4, the accumulated plastic strain for the fractured chalk with dip angles of 30° and 45° at the time 25

(a) (b)

Figure A.4: The equivalent accumulated plastic strain for the fractured chalk with dip angles of 30° (Fig. A.4a), and 45° (Fig. A.4b).

second are shown, while at this time the intact chalk has an elastic behavior.

High shear stresses cause damage and sliding of the fracture. Fracture sliding degrades the asperity angle and causes dilation (see equation A.10). Changes of the asperity angle versus time for fractures with four different dip angles is shown in Figure A.5. For fracture planes with a dip angle of 0° and 15°, the asperity angles does not change, which indicates shear stresses are small and there is no fracture sliding. At higher dip angles, increased load causes the asperity angle to decrease from its initial value of 10° to its residual value. Decreasing of the asperity angle shows the occurrence of fracture sliding and irreversible damage deformation, which is higher for materials with higher fracture dip angles.

In Figure A.6, diagram of the deviatoric stress versus the mean stress for the chalk includes a fracture with a dip angle of 30°, shows development of the stress states of the fractured chalk. The asperity angle's changes versus mean stress is included in the plot. Decreasing the asperity angle from its initial value indicates the irreversible damage progress in the fractured chalk. The behavior of the curve is elastic in the beginning. Then the slope of the curve is decreasing, which indicates the plastic deformation, while the irreversible damage(inelastic), has not started. At the point, where the irreversible damage occurs, the curve has an inflection point, at which the equivalent constitutive matrix has a sudden decrease due to the damage. When the asperity angle and consequently the irreversible damage deformation reaches to the residual value, the damage constitutive matrix does not change and the coupled constitutive model follows the trend of the elasto-plastic model. By

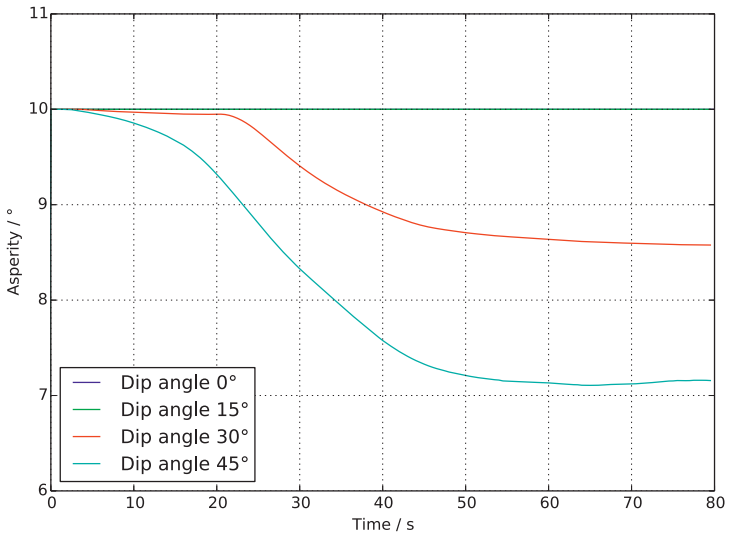

Figure A.5: Fracture asperity degradation caused by high shear stress for the fracture plane with dip angles of 0°, 15°, 30° and 45°.

increasing the compression load, subsequently the mean stress increases and this limits further shear failure. The slope of the curve then approaches the elastic curve again.

The deviatoric stresses for the chalk sample with a single fracture oriented with dip angles of 30°, 45° are demonstrated in Figure A.7. Numerical results show the deviatoric stresses are localized in the fractured plane orientation and by increasing the fracture's dip angle, the deviatoric stress increases.

A.4 Conclusion

The objective of this study was to analyze failure of fractured chalk using a continuum computational numerical model. For this purpose, a coupled elasto-plastic-anisotropic damage constitutive relation is developed and implemented to the model to describe the behavior of the fractured chalk under uni-axial loading condition. Deformation of the fracture plane is modeled with a theory of anisotropic damage model.

Plastic deformation of the chalk and irreversible deformation of the fracture are treated in a similar way by defining the plastic and damage flow rules, and using a stress return algorithm. The coupling of the plasticity and the damage models is done by making an equivalent constitutive matrix based on the total deformation

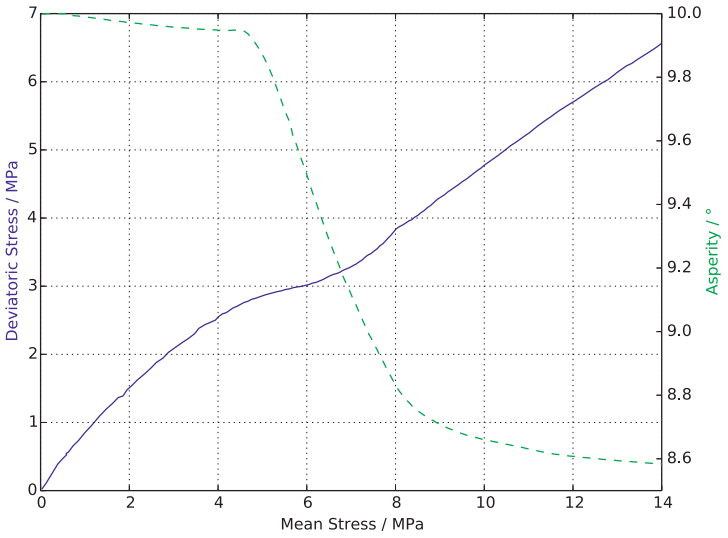

Figure A.6: Deviatoric stress and asperity angle versus mean stress, dip angle 30°

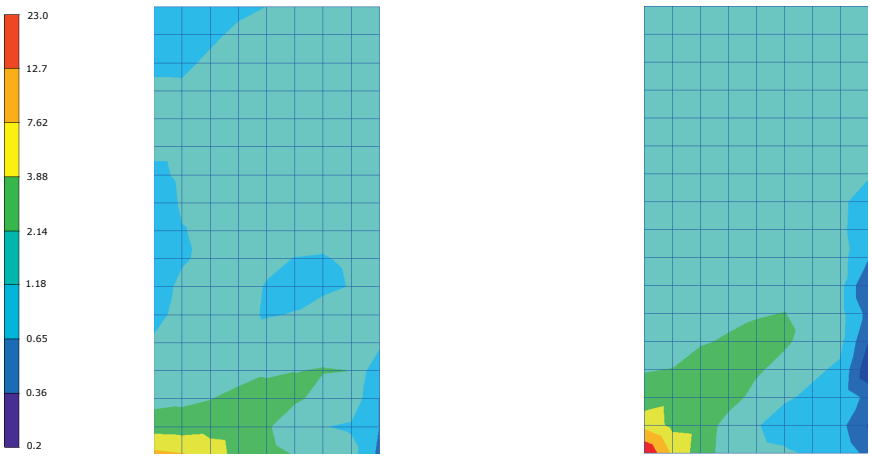

(a) (b)

Figure A.7: Deviatoric stress [MPa] for the fractured chalk with a dip angle of 30° (Fig. A.7a) and a dip angle of 45° (Fig. A.7b) : a higher dip angle creates a higher stress deviator

of the material is sum of the deformation of the intact chalk and deformation of the fracture, and both of them experience same stresses.

The developed model is validated by comparing with an analytical solution for an elastic rectangular volume with a single horizontal fracture.

Computational simulations of the coupled elasto-plastic damage show the effect of the fracture and its orientation on the overall deformation and stress distribution of the fractured chalk. Chalk tends to deform along the fracture plane, therefore in the uni-axial simulation, high deviatoric stresses are localized along the fracture plane, which facilitate the failure of the chalk.

Coupling the elasto-plastic constitutive model with the damage model shows a inflection point in the diagram of the deviatoric stress versus mean stress, at which the fracture sliding or irreversible damage started. By decreasing the asperity angle to its residual value, the slope of the curve approaches the elastic curve.

High plastic deformation along the fracture orientation, fracture sliding and decreasing of the asperity angle, can be seen for the fracture plane with dip angles of 30° and 45°.

A.5 Acknowledgments

The authors are grateful to Dr. Mohammad Nassir for his helpful discussions regarding the fracture modeling. This work is partially supported by the Research Council of Norway.

A.A Elasto-plastic Constitutive Matrix for Intact Material

Elastic constitutive matrix written as:

$$\mathsf{D}_I = \frac{E}{1+\nu}\begin{bmatrix} 1-\nu & \nu & \nu & 0 & 0 & 0 \\ \nu & 1-\nu & \nu & 0 & 0 & 0 \\ \nu & \nu & 1-\nu & 0 & 0 & 0 \\ 0 & 0 & 0 & 0.5-\nu & 0 & 0 \\ 0 & 0 & 0 & 0 & 0.5-\nu & 0 \\ 0 & 0 & 0 & 0 & 0 & 0.5-\nu \end{bmatrix} \tag{A.22}$$

where E and ν are Young's Modulus and Poisson's ratio respectively. The constitutive model of intact chalk is isotropic and symmetric.

To evaluate the irreversible part of displacement (plastic strain) a non-associated flow rule is used as follows:

$$\Delta\boldsymbol{\varepsilon}^p = \gamma^p \frac{\partial Q^p}{\partial \boldsymbol{\sigma}} \tag{A.23}$$

where γ^p is a non-negative scalar. From the theory of plasticity and consistency condition, γ^p can be found as follows [61]:

$$\gamma^p = \frac{\frac{\partial F}{\partial \boldsymbol{\sigma}}^T \mathsf{D}_I \, \Delta\boldsymbol{\varepsilon}}{\frac{\partial F}{\partial \boldsymbol{\sigma}}^T \mathsf{D}_I \, \frac{\partial Q}{\partial \boldsymbol{\sigma}} - \frac{\partial F}{\partial \kappa} \frac{\partial \kappa}{\partial \boldsymbol{\varepsilon}^p}} \tag{A.24}$$

And the elasto-plastic constitutive relation is,

$$\Delta\boldsymbol{\sigma} = \mathsf{D}^{ep} \, \Delta\boldsymbol{\varepsilon} \tag{A.25}$$

where D_{ep} is elasto-plastic constitutive matrix. and the incremental total strain $\Delta\boldsymbol{\varepsilon}$ can be split into reversible elastic and irreversible plastic strains

$$\Delta\boldsymbol{\varepsilon} = \Delta\boldsymbol{\varepsilon}^e + \Delta\boldsymbol{\varepsilon}^p \tag{A.26}$$

From mathematical manipulation and theory of plasticity, the elasto-plastic constitutive matrix $[D^{ep}]$ is obtained as the following form.

$$\mathsf{D}^{ep} = \begin{cases} \mathsf{D}_I & \text{if } \gamma^p = 0 \\ \mathsf{D}_I - \frac{\mathsf{D}_I \frac{\partial Q}{\partial \boldsymbol{\sigma}} \frac{\partial F}{\partial \boldsymbol{\sigma}}^T \mathsf{D}_I}{\frac{\partial F}{\partial \boldsymbol{\sigma}}^T \mathsf{D}_I \frac{\partial Q}{\partial \boldsymbol{\sigma}} - \frac{\partial F}{\partial \kappa} \frac{\partial \kappa}{\partial \boldsymbol{\varepsilon}^p}} & \text{if } \gamma^p > 0 \end{cases} \tag{A.27}$$

A.B Damage Constitutive Matrix

$$\mathsf{D}^{ed} = \begin{cases} \mathsf{F}_J^{-1} & \text{if } \gamma^d = 0 \\ \mathsf{F}_J^{-1} - \frac{\mathsf{F}_J^{-1} \frac{\partial Q^d}{\partial \boldsymbol{\sigma}} \frac{\partial F^d}{\partial \boldsymbol{\sigma}}^T \mathsf{F}_J^{-1}}{\frac{\partial F^d}{\partial \boldsymbol{\sigma}} \mathsf{F}_J^{-1} \frac{\partial Q^d}{\partial \boldsymbol{\sigma}} - \frac{\partial F^d}{\partial \mu} \frac{\partial \mu}{\partial \boldsymbol{\varepsilon}^p}} & \text{if } \gamma^d > 0 \end{cases} \tag{A.28}$$

The above equations are obtained from the theory of maximum damage dissipation and consistency condition, which are equivalent to the one in the plasticity model [36]. Irreversible strain of the fracture plane is obtained by using the damage flow rule and damage multiplier γ^d:

$$\Delta\boldsymbol{\varepsilon}^d = \gamma^d \frac{\partial Q^d}{\partial \boldsymbol{\sigma}} \tag{A.29}$$

A.C Transformation Matrix

$$\mathsf{T} = \begin{bmatrix} l_x^2 & m_x^2 & n_x^2 & 2\,l_x\,m_x & 2\,m_x\,n_x & 2\,l_x\,n_x \\ l_x\,l_y & m_x\,m_y & n_x\,n_y & m_x\,l_y + l_x\,m_y & n_x\,m_y + m_x\,n_y & n_x\,l_y + l_x\,n_y \\ l_x\,l_z & m_x\,m_z & n_x\,n_z & m_x\,l_z + l_x\,m_z & n_x\,m_z + m_x\,n_z & n_x\,l_z + l_x\,n_z \end{bmatrix} \tag{A.30}$$

and,

$$\left\{\begin{array}{ccc} l_x = \sin(d)\cos(a) & m_x = -\sin(d)\sin(a) & n_x = \cos(d) \\ l_y = \sin(a) & m_y = \cos(a) & n_y = 0 \\ l_z = -\cos(d)cos(a) & m_z = \cos(d)\sin(a) & n_z = \sin(d) \end{array}\right\} \tag{A.31}$$

A single fracture in a 3 -D space is defined by the dip d and strike a angles as follows:

Strike angle is the angle between true north and the line formed by intersection of the fracture plane and a horizontal plane. True north is defined by the azimuth system. In the azimuth system true north has an azimuth 0° and east has azimuth of 90°. In this work we defined azimuth of 90°.

Dip angle is angle of the inclined fracture below the horizontal plane. The dip is always measured perpendicular to the strike line.

Appendix B

Appendix B

Coupled Fluid Flow and Elasto-plastic Damage Analysis for Fractured Porous Chalk with Induced Wormhole

By Nazanin Jahani, Bjørn Haugen and Geir Berge; accepted for publication in International Journal of Rock Mechanics and Mining Sciences, DOI: 10.1016/j.ijrmms.2015.09.011

Abstract

Acid injection in a carbonate oil reservoir can increase oil recovery by etching a part of the fractured porous reservoir and generating conductive channels ("wormholes"), which creates an easier path for oil production. However, it is crucial to predict the wormhole and reservoir strength and their failure for a successful acid treatment. For this purpose, a continuum-based computational method is developed. The model includes flow in the porous chalk reservoir, flow in the wormhole and reversible and irreversible deformation of chalk and fractures, which are modeled with an equivalent elasto-plastic damage constitutive model. The coupling between the reservoir flow and the fractured chalk deformation is done by explicit coupling method. The results found that the risk of the wormhole's walls failure is higher if the natural fractures are oriented along the wormhole; however, natural fractures with larger dip angles and higher inclinations in respect to the wormhole increase the risk of the rock failure. Results shows that increased fluid production from the wormhole, which can be the result of the further acid treatments, developing irreversible behaviors of the rock and reduces the natural fracture asperity

at the wormhole's tip, in addition to increasing the wormhole's wall deformation, eventually leading to the wormhole's occlusion.

B.1 Introduction

Oil consumption in the world is going to increase dramatically while oil supply is rapidly declining. In low-permeability and low-porosity reservoirs, oil is difficult to extract by primary recovery. In this case, well stimulation techniques such as matrix acidizing are used to increase rock permeability. In matrix acidizing, acid is injected into the near-wellbore zone and reacts with the rock reservoir including natural fractures, dissolving portions of the rock and opening up existing pores and fractures [17, 18], leading to an easier oil flow by increasing the rock permeability and porosity: this allows more fluid draining to the well-bore and enhances oil production. Near-wellbore stimulation by acid is becoming increasingly important to make drilling methods more economical; however, many acidizing treatments do not produce the expected increase in reservoir productivity.

Several studies [20, 72, 24, 57] have addressed a dissolution process, leading to the formation of long, conducting and branching channels between the reservoir and the well, that can improve the porosity and permeability of carbonate reservoirs and consequently their productivity; these channels go through the rock like a worm, hence the name *wormhole* [20]. Different parameters such as the acid injection rate, fluid velocity, surface reaction rate and heterogeneity of the porous medium influence wormhole formation, and as a result the reservoir productivity [15, 31, 4, 33, 48, 58]. Such an increase in oil production due to acidizing has the negative effect of increasing the risk of rock collapse [3, 37]. In addition, stress levels around the wormhole vary during production, which can cause wormhole occlusion and wormhole failure, and influence the resulting achievement of the acid treatment. Therefore, for successful acidizing, it is crucial to predict the reservoir and wormhole strength under loading and during flow production.

For this purpose, we used a multi-physics computational model to predict the coupled phenomena that occur in the near well-bore zone of the fractured reservoir, including induced wormholes, during flow production. The schematic of the near well-bore zone is illustrated in Figure B.1. Coupling methods between reservoir flow and the rock deformation can be found in the literature [73, 55, 32, 49, 50, 71].

In this computational model the flow velocity inside the fractured porous reservoir is defined by Darcy's model, including anisotropic permeability [53, 45, 69]. To predict the reversible and irreversible deformation of the fractured chalk and wormhole, natural fractures are introduced as fractured planes in the rock material, and a continuum model [52, 51, 40, 2, 66, 67, 56, 10, 22, 13] (an equivalent constitutive model coupling reversible and irreversible deformation of chalk with

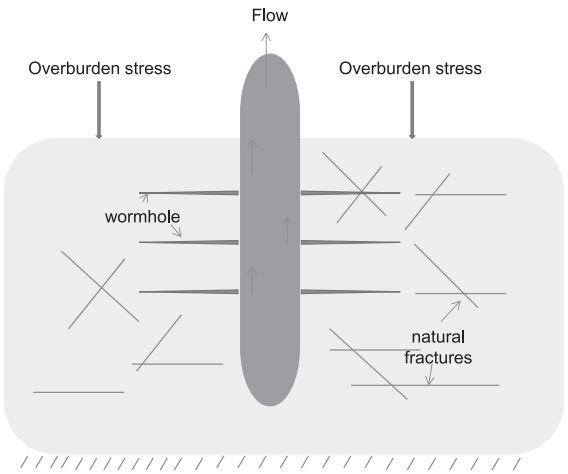

Figure B.1: Schematic of the modeled near well-bore zone, including induced wormholes and natural fractures

the reversible and irreversible deformation of the fracture plane) is applied to the computational model.

Irreversible deformation of the chalk is modeled by elasto-plastic theory [60, 59, 28] and irreversible or nonlinear deformation of the natural fractures is described by anisotropic damage theory or fracture sliding. The coupling between elasto-plastic behavior of the chalk and the nonlinear of the fracture is implemented with elasto-plastic-damage theory [36, 35, 34].

A pre-existing wormhole is introduced into the model as a channel with fluid flow. The interaction between the reservoir fluid flow and the fractured chalk deformation is done by explicit coupling method [49]. The computational method of the fluid is based on the finite-volume method, available in the in-house computational fluid dynamics (CFD) software "Brilliant", whereas the non-linear finite-element (FE) method is used to evaluate the deformation and strength of the fractured chalk, and is implemented into the "Brilliant" software [5].

B.2 Methods

This study models a part of the near well-bore area of the chalk reservoir, including one induced wormhole and natural fractures. The model for simulation study is presented in Figure B.2.

In the model, the chalk reservoir is a porous medium includes natural fractures, which are defined by their orientation in terms of azimuth and dip angles [23]. The

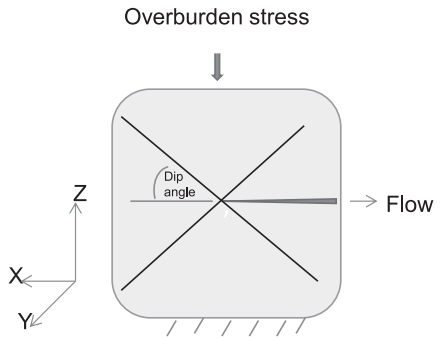

Figure B.2: Idealized representation of the near well-bore zone including wormhole and two fracture planes: the fractures and the intact chalk are modeled as an equivalent continuum model, while the wormhole is separately defined as a flow channel.

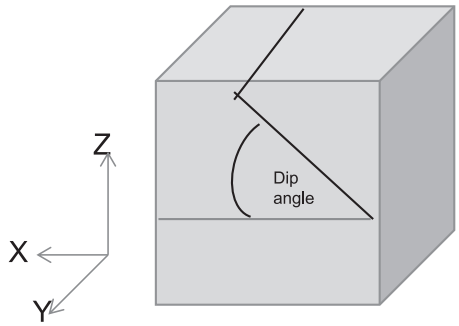

Figure B.3: Representation of one fracture plane oriented with an azimuth of 0° and a dip angle of θ.

fracture plane with a dip angle of θ and azimuth of 0° is presented in Figure B.3. The fracture plane with dip and azimuth angles of 0° is defined as a horizontal plane. The block coordinate axes are X, Y and Z, where Z is the vertical direction and X and Y axes are on the horizontal plane.

The computational model used in this study is divided into three parts:

- The fluid flow in the fractured porous medium and the wormhole;
- The geomechanical model, including both reversible and irreversible behaviors of chalk, fractures and wormhole's walls;
- The coupling between the flow and geomechanics models.

B.2.1 Flow in the Fractured Porous Rock

The flow in the fractured reservoir is modeled on Darcy scale and is formulated through the continuum approach. The Darcy velocity vector is represented by Darcy's law. By neglecting the gravity effect the Darcy velocity vector becomes:

$$\boldsymbol{q} = -\frac{\mathsf{K}}{\mu}\nabla P \tag{B.1}$$

where ∇P is the pressure gradient vector, μ is the fluid viscosity and K is the permeability of the medium and represents the directional resistance of the porous medium to the flow [23]. The permeability K can be written as a product of two components [69], the permeability scalar and the unit permeability tensor:

$$\mathsf{K} = |k|[\mathsf{k}] \tag{B.2}$$

The permeability scalar $|k|$ can be defined from the theory of laminar flow through two parallel plates separated by a narrow space:

$$|k| = \frac{w_f^2}{12} \tag{B.3}$$

where w_f is the distance between the two parallel plates, or the fracture aperture. The unit permeability tensor $[\mathsf{k}]$ is defined in compact form as:

$$[\mathsf{k}] = \delta_{ij} - n_i\, n_j \tag{B.4}$$

where δ_{ij} is the Kronecker delta; n_i and n_j are components of the normal vector to the fracture plane, $\hat{n}$. For more details see Gupta et al. [27].

The fluid velocity vector $\boldsymbol{U}$ is related to the Darcy velocity $\boldsymbol{q}$ by the chalk porosity (φ):

$$\boldsymbol{U} = \frac{\boldsymbol{q}}{\varphi} \tag{B.5}$$

In the Darcy equation, there are two unknown parameters: the velocity and the pressure gradient vectors. The velocity vector can be defined by using the mass continuity equation, which is based on the principle of conservation of mass [23].

B.2.2 Geomechanics

The geomechanical model predicts the strength and failure of the fractured chalk. In this model, the natural fractures and the intact chalk are considered as a single medium with an equivalent constitutive model, which includes both reversible and irreversible behavior of the intact chalk and natural fractures. The irreversible deformation of the intact chalk is caused by shear failure and pore collapse, and is

modeled by the theory of nonlinear plasticity; the irreversible deformation of natural fractures is modeled by the shear-dominant damage theory, and is caused by fracture sliding and fracture asperity degradation.

In this model, the constitutive models of intact chalk and natural fractures are considered separately, and a coupling method is applied to construct the equivalent constitutive model. The coupling is based on the elasto-plastic-damage model by Ibrahimbegović [36].

The equivalent constitutive Model of the Fractured Chalk

In this section the constitutive model of the intact chalk, natural fractures and their coupling are described.

Constitutive model of the intact chalk The elasto-plastic constitutive relation for the intact chalk is:

$$\Delta\boldsymbol{\sigma} = \mathsf{D}^{ep}\,\Delta\boldsymbol{\varepsilon} \tag{B.6}$$

where $\Delta\boldsymbol{\sigma}$ is the incremental stress vector and $\Delta\boldsymbol{\varepsilon}$ is the total incremental strain, which is divided into elastic (reversible) and plastic (irreversible) parts:

$$\Delta\boldsymbol{\varepsilon} = \Delta\boldsymbol{\varepsilon}^{e} + \Delta\boldsymbol{\varepsilon}^{p} \tag{B.7}$$

D^{ep} is the elasto-plastic constitutive matrix of the chalk; for an elastic chalk, D^{ep} is equal to the elastic constitutive matrix, D_I, which is a function of Young's Modulus E and Poisson's ratio ν.

D^{ep} is defined from the classical theory of plasticity [47]. The yield and potential functions of the chalk are based on the ISAMGEO chalk model presented by Plischke [60]. The chalk model includes two independent yield mechanisms: shear failure and pore collapse, where shear failure has priority over pore collapse. The shear failure yield and potential surface are defined by the Mohr-Coloumb function in stress-invariant space and as a function of chalk properties, such as cohesion c and friction angle Φ. For the potential surface, the friction angle Φ is replaced by the dilatancy angle Ψ. Chalk properties such as cohesion and friction vary during loading, which harden or soften the Mohr-Coloumb yield function. Hardening of the yield surface is applied to the model by increasing the friction angle to the peak value. After that, the material experiences pronounced softening by decreasing the cohesion and friction angles to the residual values. For the dilatancy angle Ψ, the hardening and softening are the same as for the friction angle Φ. The yield surface for pore collapse is defined by an ellipse in stress-invariant space, assuming an associated plastic flow. The parameters used in the constitutive of the chalk are listed in Table B.2.

Constitutive model of the fracture plane The fracture is modeled as a 2-D plane with a local coordinates x, y and z. The constitutive relation of the single fracture is:

$$\Delta\boldsymbol{\varepsilon}'^{d} = \mathsf{F}^{ed}\,\Delta\boldsymbol{\sigma}' \tag{B.8}$$

where $\Delta\boldsymbol{\sigma}'$ is the incremental stress of the fracture in its local coordinates, $\Delta\boldsymbol{\varepsilon}'^{d}$ is the incremental strain of the fracture (analogously to plasticity theory, it is a sum of reversible and irreversible strains), and F^{ed} is the nonlinear compliance matrix of the single fracture plane at its local coordinate. For linear deformation, F^{ed} is replaced by the linear compliance matrix F_J of the fracture plane, which takes the form:

$$\mathsf{F}_J = \begin{bmatrix} k_n^{-1} & 0 & 0 \\ 0 & k_s^{-1} & 0 \\ 0 & 0 & k_t^{-1} \end{bmatrix} \tag{B.9}$$

where k_n is the stiffness normal to the fracture plane, and k_s and k_t are the shear stiffness of the fracture plane in two orthogonal directions in the local coordinates of the fracture plane [52]. The parameters used in the constitutive model of the fracture plane are listed in Table B.2.

The nonlinear constitutive model of the fracture is modeled by assuming that its irreversible deformation is due to the frictional sliding and represented by irreversible damage theory [36, 35] in a way similar to plasticity development in chalk material by replacing the yield function with the slip function. Jing et al. [40] proposed slip and potential functions for a single fracture as follows:

$$F^d = \left[\left(\frac{\sigma'_{xy}}{\mu_x}\right)^2 + \left(\frac{\sigma'_{xz}}{\mu_z}\right)^2\right]^{\frac{1}{2}} + \sigma'_{xx} - c_f \tag{B.10}$$

$$Q^d = \left[\left(\frac{\sigma'_{xy}}{\mu_x}\right)^2 + \left(\frac{\sigma'_{xz}}{\mu_z}\right)^2\right]^{\frac{1}{2}} + \sigma'_{xx}\,\sin(\alpha) \tag{B.11}$$

where c_f is the cohesion of the fracture and μ_x and μ_z are defined as:

$$\mu_x = \tan(\Phi_r + \alpha_x) \tag{B.12}$$

$$\mu_z = \tan(\Phi_r + \alpha_z) \tag{B.13}$$

where Φ_r is the frictional angle and α_x and α_z are the asperity angles of the fractured chalk in the x and z directions. Average asperity angle, α in Equation (B.11), is the average of α_x and α_z [52].

During the irreversible deformation of the fracture, degradation of the asperity angle is observed. The asperity degradation is assumed to be a function of the

irreversible portion of the fracture displacement, which is presented in Equation (B.14).

$$\alpha_x = \alpha_{x0} \exp\left(-m \left|\varepsilon^d_{x,\text{irreversible}}\right|\right) \tag{B.14}$$

$$\alpha_z = \alpha_{z0} \exp\left(-m \left|\varepsilon^d_{z,\text{irreversible}}\right|\right) \tag{B.15}$$

and average asperity angle, α, expressed in Equation (B.16):

$$\alpha = \frac{\alpha_x + \alpha_z}{2} \tag{B.16}$$

The equivalent coupled elasto-plastic-damage model The equivalent coupled elasto-plastic-damage constitutive model is presented to demonstrate both reversible and irreversible deformation of the fractured chalk. In the equivalent coupled model the chalk and the fractured plane are modeled as two elements connected in series [56, 10]. Series models ensure that each element experiences the same incremental load, and that the total strain is equal to the sum of the strain in each element. In order to introduce an equivalent constitutive model, both fracture and chalk are defined in a same coordinate system by using a coordinate transformation [**?**]. The stress vector in each element of the series model is equal to the total stress; the linear constitutive relationship between strain and stress for the equivalent model with a single fracture is:

$$\Delta\boldsymbol{\varepsilon}^e = (\mathsf{D}_I^{-1} + \mathsf{T}^T \mathsf{F}_J \mathsf{T})\Delta\boldsymbol{\sigma} \tag{B.17}$$

where T is a transformation matrix [**?** 10], which transforms the stress vector of each block in X, Y and Z coordinate into the stress vector at the local coordinates of the fracture plane x, y and z. The equivalent compliance matrix of the elastic fractured chalk, F^t, is introduced in Equation (B.18).

$$\mathsf{F}^t = \mathsf{D}_I^{-1} + \mathsf{T}^T \mathsf{F}_J \mathsf{T} \tag{B.18}$$

The coupled equivalent elasto-plastic-damage constitutive matrix, D^t, which considers both reversible and irreversible behaviors of the fractured chalk is presented in Equation (B.19).

$$D^t = \left[(\mathsf{D}^{ep})^{-1} + (\mathsf{D}^{ed})^{-1}\right]^{-1} \tag{B.19}$$

The Permeability Update

As presented in Equation (B.3), the permeability scalar is a function of the fracture aperture. The fracture aperture varies over time because the fracture walls are not flat and parallel smooth surfaces, but contain irregularities called asperities

Figure B.4: Representation of a natural fracture with parallel walls with asperities.

Table B.1: Chalk parameters for fluid flow calculation.

Initial porosity of the medium, $\varphi_{\beta 0}$	0.4
Initial scalar value for permeability, $\lvert k \rvert$	$3.5 \times 10^{-9}\,\mathrm{m}^2$

(see Figure B.4). Asperities reduce the fluid flow and make flow velocities irregular [68]. During the shear-dominant damage of the fracture (fracture sliding), the asperity angle α degrades and aperture varies. Change of the asperity angle is a function of nonlinear fracture deformation as defined in equation (B.16). Fracture aperture variation due to the asperity angle degradation can be defined as:

$$w_f = w_{f_0}(1 - \tanh(\alpha)) \tag{B.20}$$

where w_{f_0} is the fracture aperture at the initial state and w_f is the fracture aperture at the current state, which is increased due to the asperity angle degradation. In this work, we have one fracture, and the initial value for its aperture is chosen to be $w_{f_0} = 0.25\,\mathrm{mm}$.

The Porosity Update

As mentioned earlier, the nonlinear deformation of the fracture is shear-dominant; the effect of the fracture's volume change on the fracture's porosity is neglected, hence a single-porosity approach [1] is used in the model. However, the nonlinear model of chalk considers the dilatancy effect due to shear failure and volume changes due to pore collapse. Therefore, the single porosity is updated to provide a more realistic pressure to the geomechanical model:

$$\varphi_\beta = \varphi_{\beta 0} + \boldsymbol{\varepsilon}_v \tag{B.21}$$

where φ_β and $\varphi_{\beta 0}$ are the current and the initial porosity respectively, and $\boldsymbol{\varepsilon}_v$ is the volumetric strain (compression strain is negative).

Table B.2: Chalk and fracture parameters assumed for elasto-plastic damage constitutive model.

Young's modulus, E	4000 MPa
Poisson's ratio, ν	0.22
Angle of friction for yield (initial, peak, residual), Φ	37.5°, 38°, 37.7°
Angle of friction for potential surface, Ψ	19°
Cohesion (initial, peak, residual), c	0.8 MPa, 0.8 MPa, 0.7 MPa
Fracture normal strength, k_n	30 MPa/m
Fracture shear strength, k_s, k_t	15 MPa/m, 15 MPa/m
Fracture cohesion, c_f	0
Fracture asperity angle (initial), α_x, α_z	10°, 10°
Fracture angle of friction, Φ_r	37.5°

B.2.3 Coupling Flow and Geomechanical Models

Chalk is a porous medium and pores are filled with fluid. Pore pressure is incorporated into the constitutive equation so that the total stress is subdivided into effective stress $\boldsymbol{\sigma}^{\text{eff}}$, which acts on the rock structure, and the pore pressure p [70].

$$\boldsymbol{\sigma}^{\text{eff}} = \boldsymbol{\sigma} - \alpha_{\text{Biot}}\, p \tag{B.22}$$

where α_{Biot} is called Biot's coefficient [6], which represents the ratio of the volume or water squeezed out of the rock to the total volume change for deformation at constant fluid pressure. In this work the value of α_{Biot} is constant and is equal to one. The effective stresses from Equation (B.22) are used in the constitutive relation.

The coupling between the flow model in the reservoir and solid deformation has been done by explicit or one-way coupling [49]; the flow field is a function of position, porosity and permeability from the previous increment. At each time step the flow field can be solved independently of the stress field, and the pressure gradients are solved. The stress states are evaluated once the flow field has been determined. The known pressure gradients are converted into force and used in the constitutive model to calculate the stress states.

B.2.4 Numerical Methods

In order to solve the above constitutive relations, the explicit Euler integration algorithm is applied to the nonlinear constitutive equation of the chalk and the fracture, then the return stress algorithm, proposed by Ortiz and Simo [54], is used to calculate the irreversible deformations and modify stresses and return them to the yield and slip surfaces. The return algorithm is applied separately to the constitutive models of the chalk and the fracture plane, and the irreversible deformation of each

model is calculated in two separate computations, independently of each other. At the end of each computation, stresses provided by the two models will be enforced to be equal with an additional iterative loop. The computational procedure is explained by Ibrahimbegović [36].

B.3 Model Description

The above model is applied to the section of the near well-bore area that was illustrated in Figure B.2. The geometry and boundary conditions for the computational calculations are explained in the following.

B.3.1 Geometry

Figure B.5 demonstrates the geometry and meshes for finite-element and finite-volume calculations. This computational model includes quadrilateral meshing with constant size, which are the same for finite-element and finite-volume calculations. The geometry of the model is a 3-D cuboid extending 50 cm in the X and Z directions, and 10 cm in the Y direction. The Z axis is oriented vertically. The wormhole is induced in XZ plane. The wormhole length is 25 cm and its width at the outlet is 2 cm. The natural fractures are described by their dip and azimuth angles. The case study includes two natural fractures with dip angles of θ and $-\theta$. In this study, fractures have azimuth angle 0°, and dip angles 0°, 5°, 10° and 20°.

B.3.2 Initial and Boundary Conditions

The model is under uni-axial compression loading, which represents the overburden pressure, applied on the upper surface and increasing from 1.5 MPa to 1.6 MPa in 5 seconds. The chosen time step is 0.002 seconds. The choice of the time step does not have any effects on the geomechanics simulation results; however, a larger time step impairs the stability of the flow simulation. The back-pressure at the outlet of the wormhole is assigned as a boundary condition, and the production rate is increased by reducing the back-pressure from 1.5 MPa to 1.48 MPa during the 5 seconds of the loading. The initial fluid pressure of the reservoir is 1.5 MPa.

B.4 Computational Results

In this section, the results of the finite-element and finite-volume calculations for the above model are presented. The results show the wormhole's wall and reservoir deformation and their strength during the loading and fluid production. The effect of natural fractures orientations on the stress distribution in the model are described.

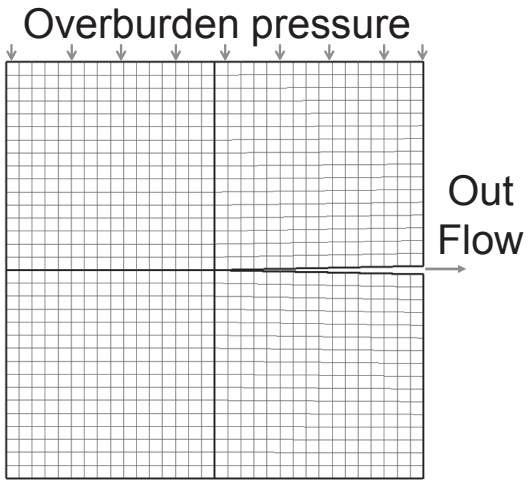

Figure B.5: The mesh used in finite-element and finite-volume calculations: the model of the fractured chalk includes a wormhole under uniaxial compressive loading.

B.4.1 Wormhole's Wall Displacement

Figure B.6 shows the vertical displacements for the fractured chalk and wormhole at time 1.5 seconds. Fractures have an azimuth of 0° and dip angles are chosen as 0°, 10° and 20°. Results indicate that the case with the fracture with a dip angle of 0° (i.e. oriented horizontally and parallel to the wormhole's axial axis) has the largest vertical displacement. By increasing the dip angle, the vertical displacement is reduced and the rock tends to move toward the fracture dipping direction. The vertical displacement causes the downward movements of the upper wormhole's wall, which is higher for the case with a lower dip angle. With time, the downward movement of the upper wormhole's wall leads to occlusion of the wormhole tip, resulting in reduced production.

B.4.2 Chalk and Wormhole Strength

Deviatoric stresses for cases with different fracture dip angles are presented in Figure B.7.

It can be seen that the deviatoric stresses are concentrated around the wormhole's walls in the case with a dip angle of 0°. The deviatoric stresses increase with the dip angle. Deviatoric stresses are concentrated around the wormhole's tip, not along the wormhole itself, but rather inclined toward the fracture dipping direction, which indicates that the fracture with higher dip angle has a dominant effect

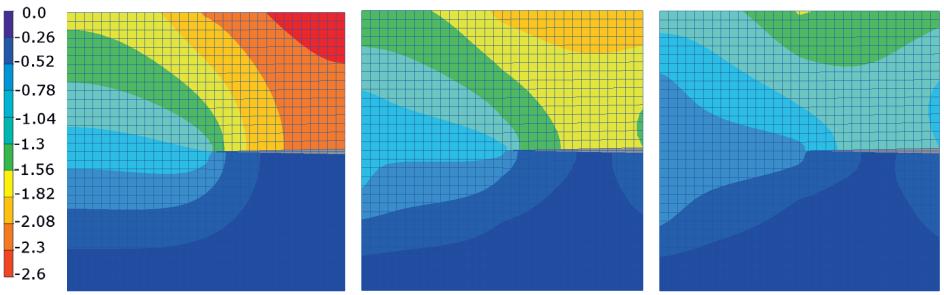

(a) Dip angle 0° (b) Dip angle 10° (c) Dip angle 20°

Figure B.6: Displacement (in mm) for the fractured chalk with various dip angles after 1.5 seconds of loading. The chalk with the fracture with a dip angle of 0° has the highest vertical displacement of the wormhole's walls, which leads to an earlier occlusion of wormhole during production.

on weakening the rock instead of the horizontal wormhole, and that the fracture oriented along the wormhole contributes to the wormhole's walls failure.

Figure B.8 shows the accumulated equivalent plastic strains for cases with fracture orientation with dip angle of 0°, 10° and 20° at time 4.6 seconds. The plastic deformation occurs earlier in the sample with a dip angle of 0° (after 3 seconds) than with a dip angle of 20° (after 4.5 seconds). Plastic deformation is concentrated around the wormhole wall at its outlet for the case including the horizontal fracture.

Figure B.9 depicts the variation of the asperity angle at the wormhole tip versus time. The asperity degrades during loading due to fracture sliding and decreases to the residual value. The plot indicates that asperity degradation occurs faster in the case with a fracture with a dip angle of 10° than in the case with zero dip angle.

B.4.3 Reservoir Depletion and Wormhole Strength

This section discusses the effect of the reservoir depletion on the wormhole's strength in a chalk with a fracture plane oriented with dip angle of 5° and azimuth angle of 0°.

Reservoir depletion is modeled by setting the back-pressure at the wormhole outlet boundary condition. The pressure difference between the wormhole outlet and the reservoir drives fluid flow out from the wormhole. The initial pressure in the chalk reservoir is 1.5 MPa. Two cases with are considered, in which the back-pressure declines over 1.5 seconds with 30 kPa and 6 kPa respectively.

The results for deviatoric stresses at simulation time of 1.5 seconds for two cases are shown in Figure B.10. Faster pressure drop in the porous chalk, which indicates faster reservoir depletion, leads to higher pressure gradients and hence

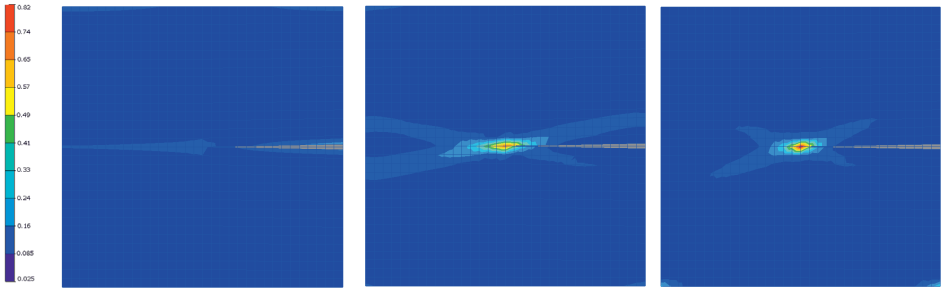

(a) Dip angle 0° (b) Dip angle 10° (c) Dip angle 20°

Figure B.7: Deviatoric stresses (MPa) for the fractured chalk with various dip angles after 1.5 seconds of loading: stress concentrates along the fracture dipping direction.

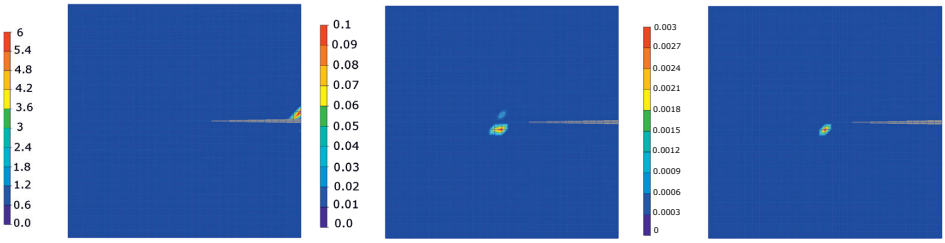

(a) Dip angle 0° (b) Dip angle 10° (c) Dip angle 20°

Figure B.8: Equivalent plastic strain ($\times 10^3$) for the fractured chalk: The accumulated plastic deformation is higher in the sample with a lower dip angle.

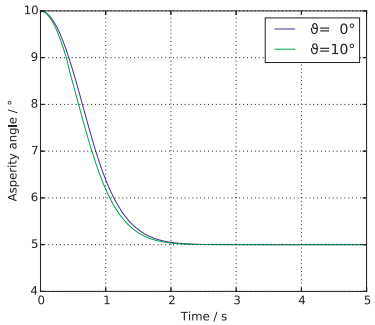

Figure B.9: Asperity variation versus time at the wormhole tip: Degradation is faster for the case with a larger dip angle.

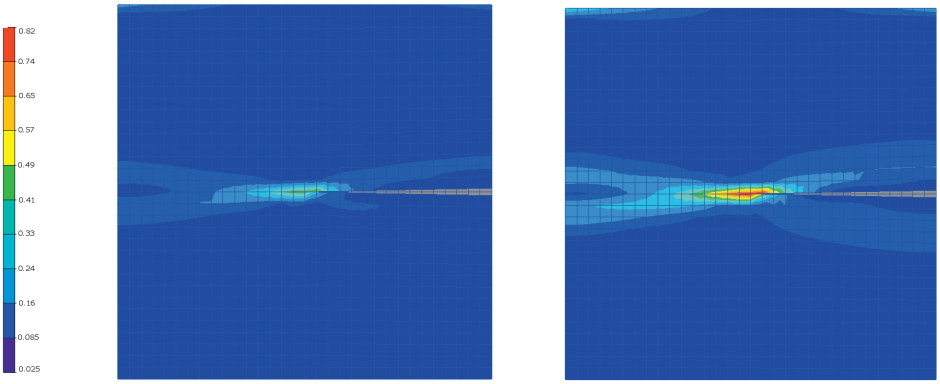

(a) Slow reservoir depletion: 6 kPa pressure drop at the boundary outlet in 1.5 seconds.

(b) Fast reservoir depletion: 60 kPa pressure drop at the boundary outlet in 1.5 seconds.

Figure B.10: Deviatoric stresses (MPa) at time 1.5 seconds, seconds for two cases with different back-pressure boundary conditions.

higher stresses in the porous medium. As a result of the high deviatoric stresses, damage and asperity degradation grow faster. The asperity angle distribution in Figure B.11 indicates a higher degradation around wormhole's tip in the case with faster pressure drop. The initial asperity angle is 10° and the lower angles around the wormhole indicate asperity degradation.

As mentioned, degradation of the asperity angle increases the permeability by opening the fracture aperture; however, simulation results indicate that the flow flux enhancement from the wormhole's outlet due to the asperity degradation is insignificant, and for the cases including a fracture with dip angles of 0° and 5° the flow flux enhancement is less than 1 %.

B.5 Conclusion

In this work, an equivalent coupled elasto-plastic damage model for fractured chalk including wormholes is developed and coupled with fluid flow and implemented in CFD-FE code. This is done to study the effects of the loading and existence of natural fractures on the strength and deformation of wormholes and chalk during production from naturally fractured reservoirs. Although wormholes can make an easier path for the flow, they might also collapse and thereby neutralize their effect on recovery.

Results show that the orientation of the wormhole plane with respect to the orientation of the natural fracture planes plays an important role on rock strength

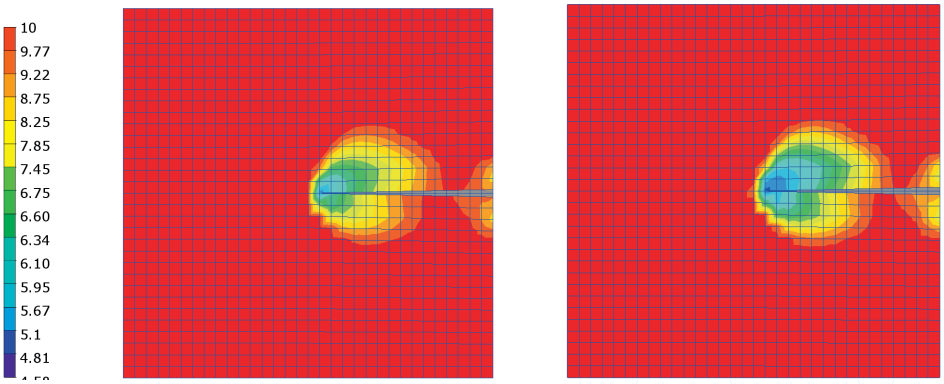

(a) Slow reservoir depletion: 6 kPa pressure drop at the boundary outlet in 1.5 seconds.

(b) Fast reservoir depletion: 30 kPa pressure drop at the boundary outlet in 1.5 seconds.

Figure B.11: Asperity angle (degree) distribution in the porous chalk at time 1.5 seconds for two cases with different back-pressure boundary conditions.

and, consequently, flow production. The orientation of natural fractures has a strong effect on overall reservoir deformation. In the case of uni-axial compressive load, the high vertical deformation of the chalk with a horizontal fracture plane causes high downward movement of the wormhole's wall, which can lead to wormhole occlusion. Furthermore, the fracture orientation relative to the wormhole has a strong impact on the wormhole's failure and damage around it; the wormhole's wall experiences high irreversible deformations in the case with the horizontal fracture.

In contrast, damage development and the fracture's asperity degradation around the wormhole increases permeability by opening the fracture aperture; however, results indicate an insignificant effect on the production rate.

Increasing the pressure differences between the outlet boundary and the reservoir increases the overall deformation of the chalk, increases the risk of the chalk and wormhole failure, and thereby wormhole occlusion.

B.6 Acknowledgments

We would like to thank Petrell AS, the Research Council of Norway, BP Norge AS and Norwegian University of Science and Technology (NTNU) for their financial support.

Appendix C

Appendix C

Effects of Natural Fracture Orientations on Porosity Evolution and Stress States of the Acidized Rock: Computational Simulation with Coupled Flow and Elastic Material

By Nazanin Jahani, Bjørn Haugen and Geir Berge; submitted to the *Journal of Petroleum Science and Engineering*.

Abstract

Acid injection in a low permeability carbonate oil reservoir can increase the oil recovery by etching a part of the medium; creating a conductive channel and consequently increasing the mass transfer and oil production. Heterogeneity of the porous carbonate reservoir influences the dissolution pattern and formation of the conductive channel, which is called a wormhole. In order to understand these effects, a computational model has been developed to simulate the acid transport in the porous media and dissolution of the fractured chalk. The natural fractures affect the dissolution pattern by directing the flow potential along the fractures. The results found that in a chalk core sample with a vertical fracture plane, which is orientated parallel to the plane between the inlet and the core, the injected acid has the best penetration depth through the core sample. However, the vertical fracture

leads to high deviatoric stresses in the core, which can result in an earlier failure of the material, thus a negative effect on the oil recovery.

C.1 Introduction

With low permeability and porosity reservoirs, oil is trapped in the rock and cannot be extracted by initial drilling. Therefore, well stimulation techniques such as fracturing is used to increase the permeability of the carbonate rock. Two ways of well stimulation are fracturing and matrix acidizing. During the fracturing, fluid is injected at higher pressure than reservoir pressure. The high reservoir's pressure leads to the fracture opening new channels. In matrix acidizing, acid is injected at a lower pressure than the matrix pressure and acid reacts with the carbonate rock, dissolving portion of the rock and opening up the existing spaces which leads an easier oil flow by increasing the rock permeability and porosity. This allows more fluid draining to the well-bore and enhances oil production. Well stimulation by acid is becoming increasingly important to reduce the drilling costs. However, many acidizing treatments do not produce the expected increase in reservoir productivity. Several studies [24, 57] have addressed a dissolution process, which leads to the formation of a long, conducting and branching channel between the reservoir and the well, can improve the porosity and permeability of the carbonate reservoir and consequently its productivity. This channel goes through the rock like a worm, hence the name "wormhole". Several experimental works [15, 31, 20, 4, 33, 48], and numerical studies such as [25, 26, 43, 44, 58, 57, 11, 46] have been conducted to understand the effect of parameters such as the acid injection rate, fluid velocity, surface reaction rate and properties of the media on the channel structure. However, the effect of the heterogeneity of the porous media due to the random orientation of its natural fractures have not been related to the rock dissolution processes. In addition, the dissolution process impacts on the overall deformation and strength of the rock due to the changes to the fluid pore pressure, which affect the flow production and again influences the overall effect by the acid treatment. The goal in this work is to relate the effect of the fracture orientations to the dissolution pattern and understand the effects of different dissolution patterns on the rock strength. For this purpose a continuum multi-physics computational model is developed to describe the acid flow into the porous chalk core sample including natural fractures. Simulation predicts the porosity evolving due to the chalk dissolution by the injected acid and relates the dissolving pattern to the fracture orientations. In addition, the influences of the dissolution pattern on the stress distribution in the chalk core are investigated.

C.2 Physical Model

The first part of this section describes a physical model that accounts for the acid flow and chalk dissolution. The model is based on continuum equations written on Darcy scale [16]. The second part, describes a geomechanical model integrated with a flow model that accounts for the strength of the acidized fractured rock.

C.2.1 Model for Chalk Dissolution

Acid flows by convection into pore spaces. The acid molecules are transfered to the surface of pores and acid reacts with the rock and the reaction products transfer back to the bulk of the flowing acid. As a result of the reaction, porosity evolves and causes an easier path for the flow. A mathematical description of acid transport in fractured porous medium is presented by Golfier et al. [25] by considering the following assumptions.

1. The reaction products, which transfer back to the bulk, are very small thus it is assumed they do not change the total fluid mass.

2. The interface shape changes is slow.

3. This model is considered as a mass transfer controlled regime; it is assumed the reaction is very fast and the acid concentration at the fluid-solid phase is negligible.

Flow Processes

Darcy velocity is defined according to Darcy's law. Darcy velocity for a laminar single-phase fluid flow with neglecting the gravity effect is presented in Equation (C.1).

$$\mathbf{q} = -\frac{1}{\mu}\mathbf{K} \cdot \vec{\nabla} P \tag{C.1}$$

where P is the pressure and $\vec{\nabla} P$ is the pressure gradient; $\mathbf{K}$ is permeability tensor [27] and defined in Equation (C.3). The fluid velocity vector $\mathbf{U}$ is related to the Darcy velocity q by the porosity (φ)

$$\boldsymbol{U} = \frac{\boldsymbol{q}}{\varphi} \tag{C.2}$$

$$\mathbf{K} = |k|\, k_{ij} \tag{C.3}$$

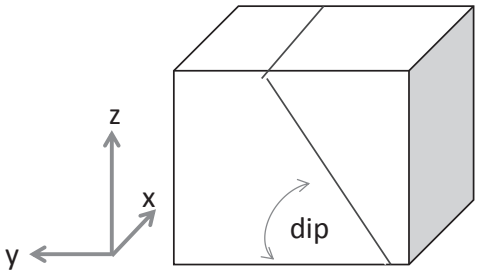

Figure C.1: An illustration of a Fracture plane with dip angle d and azimuth 90°

The permeability tensor **K** is the product of two components: the tensor part k_{ij} and permeability scalar $|k|$. The tensor k_{ij} shows the directional effect in the fluid flow due to the existence of the fractures in the porous medium and defined as:

$$k_{ij} = \delta_{ij} - n_i\, n_j \tag{C.4}$$

where, n_i and n_j are the components of the vector normal to the fracture plane, projected to the fracture plane coordinate axes; δ_{ij} is the Kronecker delta.

Fracture orientation is determined by the azimuth a and dip angles d. The dip angle is the angle of the inclined fracture below the horizontal plane and the azimuth angle is the angle of the intersection line of the fracture plane and a horizontal plane with the positive x axis. A fracture plane with an azimuth of 90° and a dip angle is illustrated in figure (C.1).

The permeability scalar $|k|$ accounts for the intensity of the anisotropy due to the presence of fractures in the porous medium. The permeability scalar $|k|$ can be expressed as:

$$|k| = \frac{2}{3} f\, w_f^3 \tag{C.5}$$

where f is the number of the fracture in a sample and w_f is half of the fracture aperture and is the perpendicular distance between the parallel walls of a fracture.

Continuity Equation

The continuity equation is based on the principle of conservation of mass,

$$\frac{\partial \rho\, \varphi}{\partial t} + \vec{\nabla} \cdot \mathbf{U} = 0 \tag{C.6}$$

where φ represent porosity of the rock.The continuity equation leads to the following form for incompressible flow by making an assumption that the process is in steady-state due to the slow change in the interface shape.

$$\vec{\nabla} \cdot \mathbf{U} = 0 \tag{C.7}$$

Table C.1: Pore scale data, used in the Darcy model

Stoechiometric coefficient, β	1.37
Local mass transport, α_c	$10\,\mathrm{s}^{-1}$
Chalk density, ρ_R	$2499\,\mathrm{kg\,m}^{-3}$
Scalar value of permeability, $\|k\|$	$10^{-10}m^2$
Initial porosity, φ	0.4

Transport Equation

The transport equation is derived by balancing of all mass fluxes across the system. Here, convection and dispersion determine the transport process of fluid in the porous media. The transport equation is applied to all materials in the system. For example, the transport equation for acid in the porous media is approximated as:

$$\varphi\frac{\partial C_a}{\partial t} + \mathbf{U}\cdot\vec{\nabla}C_a = \vec{\nabla}\cdot(\varphi\mathbf{D_e}\cdot\vec{\nabla}C_a) - \alpha_c(C_a) \tag{C.8}$$

The first three terms in the equation represent accumulation, convection and dispersion of the acid, respectively. The forth term is defined as a sink or the acid consumption term and describes the depletion of acid due to the reaction; D_e is the dispersion tensor and α_c is the local mass transfer coefficient, which are obtained from the pore scale models and used as inputs to the Darcy model. The pore scale parameters obtained from Golfier et al. [24] and listed in Table C.1 (for more detail see: [25, 62]). In this work the effect of heterogeneity of the porous media for defining the dispersion tensor is not considered.

Dissolution

The amount of solid dissolved, which causes porosity evolution, is equivalent to the amount of acid consumed; The evolution of the porosity field is defined by using the stoichmietry of the reaction as:

$$\frac{\partial\varphi}{\partial t} = \frac{\beta\,\alpha_c C_a}{\rho_R} \tag{C.9}$$

where ρ_R is the rock density, β represents the stoechiometric coefficient of the chemical reaction. The resulting acid concentration profile from Equation(C.8) is used to solve the dissolution equation to find the new porosity field.

C.2.2 Model for Prediction of Chalk Strength

The concept of *equivalent continuum* is used in order to model the fractured chalk. In this method the chalk including discontinuity is treated as a single medium with

an equivalent constitutive model.

Constitutive Model for Fractured Chalk

The equivalent constitutive model for the chalk with a single fracture is written as follows:

$$\Delta\boldsymbol{\varepsilon}^t = \mathsf{F}^t \Delta\boldsymbol{\sigma}^t \tag{C.10}$$

where, $\boldsymbol{\varepsilon}^t$ is the total strain vector and is equal to the sum of the strain in the fracture and the intact chalk. $\boldsymbol{\sigma}^t$ is the total stress vector and is equal to the stress of the fracture and the intact chalk [22]. F^t is the equivalent compliance matrix of the elastic fractured chalk:

$$\mathsf{F}^t = \mathsf{F}_I + \mathsf{T}^T \mathsf{F}_J \mathsf{T} \tag{C.11}$$

where F_I is the elastic compliance matrix of the chalk without fracture and F_J is the compliance matrix of the elastic fracture plane in its local coordinates:

$$\mathsf{F}_I = \mathsf{D}_I^{-1} \tag{C.12}$$

$$\mathsf{D}_I = \frac{E}{1+\nu}\begin{bmatrix} 1-\nu & \nu & \nu & 0 & 0 & 0 \\ \nu & 1-\nu & \nu & 0 & 0 & 0 \\ \nu & \nu & 1-\nu & 0 & 0 & 0 \\ 0 & 0 & 0 & 0.5-\nu & 0 & 0 \\ 0 & 0 & 0 & 0 & 0.5-\nu & 0 \\ 0 & 0 & 0 & 0 & 0 & 0.5-\nu \end{bmatrix} \tag{C.13}$$

where E and ν are Young's Modulus and Poisson's ratio respectively.

$$\mathsf{F}_J = \begin{bmatrix} k_n^{-1} & 0 & 0 \\ 0 & k_s^{-1} & 0 \\ 0 & 0 & k_t^{-1} \end{bmatrix} \tag{C.14}$$

where k_n is the stiffness normal to the fracture plane, and k_s and k_t are the shear stiffness of the fracture plane in two orthogonal directions [52]. The constitutive of the fracture plane is written in its local coordinate plane (x', y', z') and the axis of x' is the axis normal to the fracture plane. The block coordinate systems is defined by axes of x, y and z, which is illustrated in figure (C.1)). T is a 6×3 transformation matrix [10**?**] that transforms the stress vector of the fracture plane into the stress vector at the block coordinates as follows:

$$\begin{Bmatrix} \sigma'_{xx} & \sigma'_{xy} & \sigma'_{xz} \end{Bmatrix}^T = \mathsf{T} \begin{Bmatrix} \sigma_{xx} & \sigma_{yy} & \sigma_{zz} & \sigma_{xy} & \sigma_{yz} & \sigma_{xz} \end{Bmatrix}^T \tag{C.15}$$

$$\mathsf{T} = \begin{bmatrix} l_x^2 & m_x^2 & n_x^2 & 2\,l_x\,m_x & 2\,m_x\,n_x & 2\,l_x\,n_x \\ l_x\,l_y & m_x\,m_y & n_x\,n_y & m_x\,l_y + l_x\,m_y & n_x\,m_y + m_x\,n_y & n_x\,l_y + l_x\,n_y \\ l_x\,l_z & m_x\,m_z & n_x\,n_z & m_x\,l_z + l_x\,m_z & n_x\,m_z + m_x\,n_z & n_x\,l_z + l_x\,n_z \end{bmatrix} \tag{C.16}$$

Table C.2: Chalk and fracture parameters used for analyses

Young's modulus, E	4000 MPa
Poisson's ratio, ν	0.22
Fracture normal strength, k_n	30 MPa/m
Fracture shear strength, k_s, k_t	15 MPa/m, 15 MPa/m
Biot's coefficient α_{Biot}	1

and

$$\begin{Bmatrix} l_x = \cos(x', x) & m_x = \cos(x', y) & n_x = \cos(x', z) \\ l_y = \cos(y', x) & m_y = \cos(y', y) & n_y = \cos(y', z) \\ l_z = \cos(z', x) & m_y = \cos(z', y) & n_y = \cos(z', z) \end{Bmatrix} \tag{C.17}$$

For the porous chalk including flow with pore pressure p, $\boldsymbol{\sigma}^t$ is replaced by the effective stress $\boldsymbol{\sigma}^{t\prime}$ as follows:

$$\boldsymbol{\sigma}^{t\prime} = \boldsymbol{\sigma}^t - \alpha_{\text{Biot}}\, p \tag{C.18}$$

where α_{Biot} is the Biot's coefficient. Parameters of the constitutive model are listed in Table C.2.

C.3 Computational Simulation

The above physical model is implemented to an in-house computational code [5]. The computational method of the fluid is based on Finite-Volume method, whereas the Finite Element method is used to evaluate the stress states of the rock. The known pressure gradients from the fluid flow model converts to the force and used in the constitute model to calculate the stress states. The fluid pore pressure is used to calculate the effective stresses.

C.3.1 Results

The chalk heterogeneity due to the random orientation of the natural fractures affects the dissolution pattern and influences the rock strength. The aim of this study is to understand the effect of the fracture orientation on the dissolution pattern, porosity development and stress states of the acidized chalk. For this reason computational simulations for the three chalk cores including a single fracture of different orientations have been done. The coordinate axes are depicted in figure C.1.

1. Case 1: azimuth 90° and dip 0°; the fracture plane is parallel to the horizontal plane xy.

2. Case 2: azimuth 90° and dip 15°, which is inclined 15° from the horizon.

3. Case 3: azimuth 90° and dip 90°, which is oriented vertically and parallel to the xz plane.

The model consists of a rectangular volume of 2 cm in vertical direction, z, and 1 cm in horizontal, x and y directions. Displacement for faces normal to x and y directions are zero in their normal directions. The bottom surface has zero displacement in z direction.

Acid is injecting for 10 seconds from the middle of the top surface of the chalk core. The initial pore pressure is 0.08 MPa. Acid mass fraction is given as an inlet boundary conditions. The simulation runs for 15 seconds, under uniaxial compression load; compression boundary load is applied on the top surface and is increasing linearly from 0.09 MPa to 0.45 MPa for 8 seconds and they remains constant from 8 to 15 seconds.

The injected acid is at low concentrations, therefore physical properties of water is used for the numerical simulation.

Dissolution Pattern

For the same amount of the injected acid, the acid mass fraction distribution (see Figure C.2) and the porosity development (see Figure C.3) are evaluated for the chalk samples with mentioned fracture orientations; The acid concentration profile is related to the directional effect of the fractures on the flow and is characterized in the following.

In Figure C.2a, the acid spread over the surrounding of the core sample in the horizontal directions. The penetration depth of acid is restricted to the region close to the inlet. The porosity field at the specific time is depicted in Figure C.3a.

In Figure C.2b, the acid penetrates into the core sample, however with orientation toward the surrounding. The resulting porosity fields is illustrated in Figure C.3b.

Figure C.2c illustrates that the acid penetrates into the core sample and a longer and deeper channel in compare to case 1 and 2 is formed. The porosity is evolved along the core sample, (see Figure C.3c).

Vector of Velocity and Pressure Distribution

Figure C.4 shows the velocity vectors and the pressure distribution for the mentioned three cases. As it can be seen the vector of velocity is along the fracture plane. In case 1 including the horizontal fracture, fluid remains close to the inlet, thus the fluid pressure is increasing around the inlet, which leads to a high pressure gradient around the inlet. In case 2 including the inclined fracture plane, the fluid

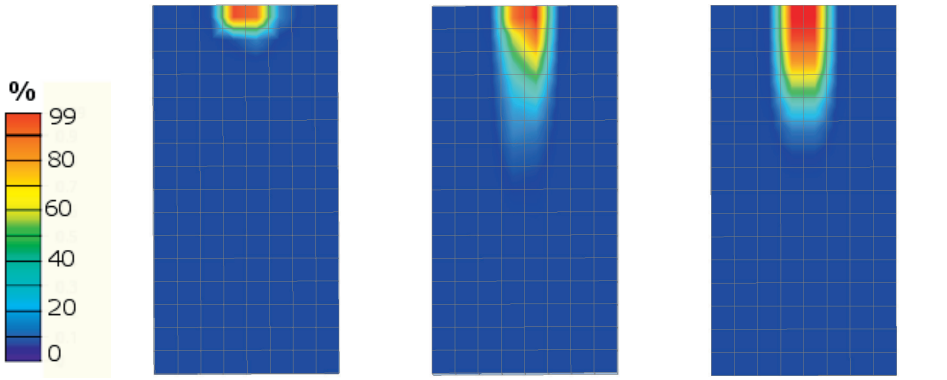

(a) case 1 includes a horizontal fracture

(b) case 2 includes a 15° inclined fracture

(c) case 3 includes a vertical fracture

Figure C.2: Acid mass fraction distribution in the middle of the core samples, yz plane, at time 8 seconds

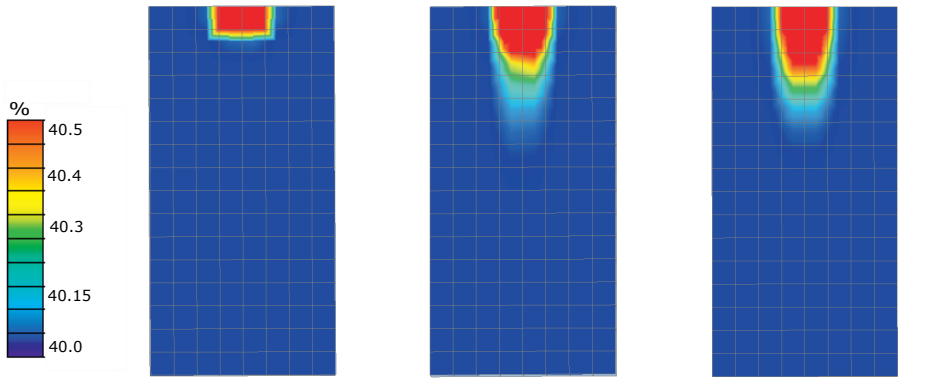

(a) case 1 with a horizontal fracture

(b) case 2 with a 15° inclined fracture

(c) case 3 with a vertical fracture

Figure C.3: Porosity profiles in the middle of the core samples, yz plane, at time 8 seconds

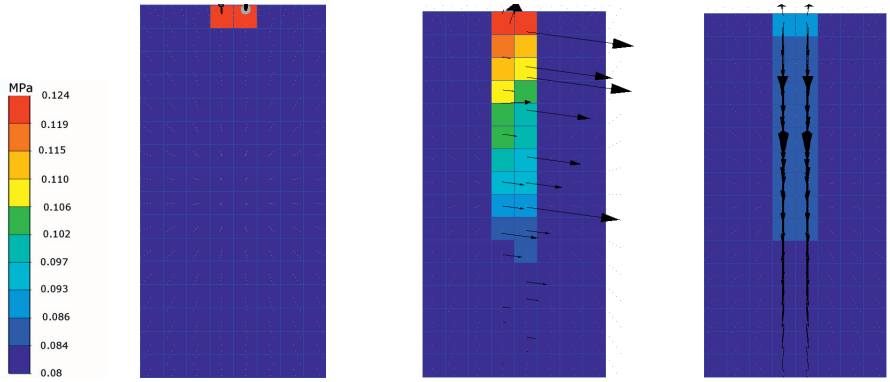

(a) case 1 with a horizontal fracture

(b) case 2 with a 15° inclined fracture

(c) case 3 with a vertical fracture

Figure C.4: Pressure profiles and velocity vectors in the middle of the core samples, yz plane, at time 8 seconds

can flow through the core along the fracture direction, which leads the inclined flow direction. In case 3, the fluid flows along the vertical fracture plane, resulting to a deep penetration inside the core and a homogeneous pressure distribution.

Stress Distribution

In Figure C.5, deviatoric stresses, J, for a plane in the middle of the core sample, parallel to yz plane, at time 8 seconds is depicted. In cases 1 and 2, the stresses are lower around the inlet. Because the higher pressure around the inlet leads to a lower effective stresses. In case 2, high deviatoric stresses are concentrated along the fracture plane at the bottom of the core sample. In case 3, the stress distribution is uniform, however the core sample experiences an overall higher stresses in compare to case 1 and 2.

C.4 Conclusion

A 3-D computational coupled flow and stress model has been presented in this paper in order to relate the effect of the natural fractures on the dissolution patterns, which is formed by the acid injection into the chalk core sample. Also the impact of different dissolution patterns on the chalk strength is studied. In this model the transport and reaction on Darcy scale are included in the flow model. An Equivalent continuum model, which includes the constitutive model of the both intact chalk and fracture plane is applied into the stress model. Several simulations have

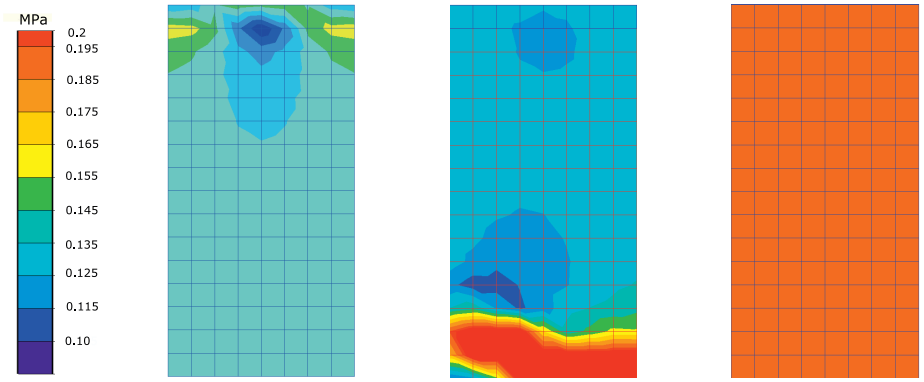

(a) case 1 with a horizontal fracture

(b) case 2 with 15° inclined fracture

(c) case 3 with a vertical fracture

Figure C.5: Deviatoric stresses J in the middle of the core samples, yz plane, at time 8 seconds

been performed on the acidized chalk core sample including the different oriented fracture plane. Results show the chalk sample with the fracture plane oriented with azimuth 90° and dip of 90°, which is orientated parallel to the vertical plane has the best penetration depth through the chalk core sample, therefore it can improve the fluid production. In contrast, the deviatoric stresses for the case includes a vertical fracture is higher than cases with horizontal fracture and with a low dip angle fractures. This can cause an earlier shear failure in the chalk and neutralize their effect on having an improved flow production. The deviatoric stress is lower in the core sample with a dip angle of 0°, however the acid remains around the inlet and cannot flow inside the core results high acid concentration around the inlet and etching a large portion of the chalk around the inlet area, which leads to a weaker structure and increase the risk of the failure.

C.5 Acknowledgments

We would like to thank Petrell As, the Research Council of Norway, BP Norge AS and Norwegian University of Science and Technology (NTNU) for their financial support.

Bibliography

Bibliography

[1] M. Bagheri and A. Settari. Modeling of geomechanics in naturally fractured resrvoirs. *SPE Reservoir Evaluation & Engineering*, 2008.

[2] M.A. Bagheri and A. Settari. Effects of fracture on reservoir deformation and flow modeling. *Can. Geotech.*, 43:574–586, 2006.

[3] A. Bauer, L. E. Walle, J. Stenebraaten, and E. Papamichos. Impact of acidizing-induced wormholes in chalk on rock strength. In *47th US Rock Mechanics-Geomechanics Symposium. San Franscisco: ARMA*, 2013.

[4] B. Bazin. From matrix acidizing to acid fracturing: A laboratory evaluation of acid/rock interactions. In *SPE 66566*, 2001.

[5] Geir Berge. Brilliant computational fluid dynamics, 2000. URL `http://www.brilliant-cfd.com/`.

[6] Maurice A. Biot. General theory of three dimensional consolidation. *Journal of applied Physics*, 12(2):155–164, 1941.

[7] Ignacio Carol, Egidio Rizzi, and Kasper Willam. On the formulation of anisotropic elastic degradation, 1. theory based on a pseudo-logarithmica damage tensor rate. *International Journal of Solid and Structures*, 38:491–518, 1999.

[8] Ignacio Carol, Egidio Rizzi, and Kasper Willam. On the formulation of anisotropic elastic degradation, 2. generalized pseudo-rankine model for tensile damage. *International Journal of Solid and Structures*, 38:519–546, 1999.

[9] L. Chen, J.F. Shao, and H.W. Huang. Coupled elasoplastic damage modeling of anisotropic rocks. *Computer and Geotechnics*, 37:187–194, 2010.

[10] T. F. Cho, M. E. Plesha, and B. Haimson. Continuum modelling if jointed porous rock. *International Journal for Numerical and Analytical Methods in Geomechanics*, 15:333–353, 1991.

[11] Charles Edouard Cohen, Didier Ding, Michel Quintard, and Brigitte Bazin. From pore scale to wellbore scale: Impact of geometry on wormhole growth in carbonate acidization. *Chemical Engineering Science*, 63:3088–3099, 2008.

[12] D. Robert Cook, S. David Malkus, E. Michael Plesha, and J. Robert Witt. *Concepts and Application of Finite Element Analysis*. Wiley India, fourth edition, 2003.

[13] N. G. W. Cook. Natural joints in rock: Mechanical, hydraulic and seismic behaviour and properties under normal stress. *International Journal of Rock Mechanics and Mining Sciences*, 29(3):198–223, 1992.

[14] C. Crowe, J. Masmonteil, and R. Thomas. Trend in matrix acidizing. *Oil field review*, pages 24–40.

[15] G. Daccord, E. Touboul, and R. Lenormand. Carbonate acidizing: Toward a quantitative model of the wormholing phenomenon. *SPE Production Engineering*, 1989.

[16] P. Dietrich, R. Helmig, M. Sauter, H Hoetzl, J. Koengeter, and G. Teutsch. *Flow and Transport in Fractured Porous Media*. Springer, 2005.

[17] C. Dong, A. Hill, and D. Zhu. Acid etching patterns in naturally-fractured formations. In *SPE 56531*, October 1999.

[18] C. Dong, D. Zhu, and A.D. Hill. Acid penetration in natural fracture networks. In *SPE 78791*, 2002.

[19] Joel H. Ferziger and Milovan Peric. *Computational Methods for Fluid Dynamics*. Springer, 2002.

[20] H. S. Fogler and C. N. Fredd. Influence of transport and reaction on wormhole formation in porous media. *AIChE Journal*, 44(9):1993–1949, 1998.

[21] C. N. Fredd and H. S. Fogler. Optimum conditions for wormhole formation in carbonate porous media: Influence of transport and reaction. *SPE Journal*, 4:196–205, 1999.

[22] C.M. Gerrard and G.N. Pende. Numerical modelling of rainforced jointed rock masses, i. theory. *Computer and Geotechnics*, 1:293–318, 1985.

[23] T.D. Van Golf-Racht. *Fundamentals of fractured reservoir engineering*, volume 12. Elsevier, 1982.

[24] F. Golfier, B. Bazin, C. Zarcone, R. Lenormand, D. Lasseux, and M. Quintard. Acidizing carbonate reservoir: Numerical modelling of wormhole propagation and comparison to experiments. In *SPE 68922*, 2001.

[25] F. Golfier, C. Zarcone, B. Bazin, R. Lenormand, D. Lasseux, and M. Quintard. On the ability of a darcy-scale model to capture wormhole formation during the dissolution of porous medium. *J. Fluid Mech*, 457:213–254, 2002. doi: 10.1017/S0022112002007735.

[26] F. Golfier, B. Bazin, R. Lenormand, and M. Quintard. Core-scale description of porous media dissolution during acid injection part i: Theoretical development. *Computational and Applied Mathematics*, 23(2-3):173–194, 2004.

[27] A. Gupta, G. Penuela, and R. Avila. An integrated approach to the determination of permeability tensor for naturally fractured reservoirs. *Journal of Canadian Petroleum Technology*, 12(40):43–48, 2001.

[28] J. Randall Hickman. *Formulation and Implementation of a Constitutive Model for Soft Rock*. PhD thesis, Virginia Polytechnic Institute and State University, September 2004. Chapter 4: Review of Proposed Constitutive Models for Chalk.

[29] R. J. Hickman, M. S. Gutierrez, V. De Gennaro, and P. Delage. A model for pore-fluid-sensitive rock behavior using a weathering state parameter. *International Journal for Numerical and Analytical Methods in Geomechanics*, 32 (16):1927–1953, 2008. doi: 10.1002/nag.703.

[30] R. Hill. *The Mathematical Theory of Plasticity*. Clarendon Press, Oxford, 1950.

[31] M.L. Hoefner and H. S. Fogler. Pore evolution and channel formation during flow and reaction in porous media. *AIChE Journal*, 34(1):45–54, 1988.

[32] Litang Hua, H. Philip Winterfeld, Perapon Fakcharoenphol, and Yu-Shu Wu. A novel fully-coupled flow and geomechanics model in enhanced geothermal reservoirs. *Journal of Petroleum Science and Engineering*, 107:1–11, 2013.

[33] T. Huang, A.D. Hill, and R.S. Schechter. Reaction rate and fluid loss: The keys to wormhole initiation and propagation in carbonate acidizing. *SPE Journal*, 5(3), 2000.

[34] A. Ibrahimbegović and D. Marković. Complementary energy based fe modelling of coupled elasto-plastic and damage behavior for continuum microstructure computations. *Computer methods in applied mechancis and engineering*, (195):5077–5093, 2006.

[35] A. Ibrahimbegović, D. Marković, and F. Gatuingt. Constitutive model of coupled damage-plasticity and its finite element implementation. *Revnue europeenne des elements finis.*, 12(4):381–405, 2003.

[36] Adnan Ibrahimbegović. *Nonlinear Solid Mechanics, Theoretical Formulation and Finite Element Solution Methods*. Springer, 2009.

[37] N. Jahani, G. Berge, and B. Haugen. Prediction of rock strength with matrix acidizing stimulation and induced wormhole by computational simulation methods. In *Rock Engineering and Rock Mechanics: Structures in and on Rock Masses*, page 1291 1294. CRC Press, 2014. doi: 10.1201/b16955-224.

[38] L. Jing. A review of techniques, advances and outstanding issues in numerical modelling for rock mechancis and rock engineering. *International journal of Rock Mechanics and Mining Science*, 40:283–353, 2003. doi: 10.1016/S1365-1609(03)00013-3.

[39] L. Jing and J.A. Hudson. review paper numerical methods in rock mechancis. *International journal of Rock Mechanics and Mining Science*, 39:409–427, 2002.

[40] L. Jing, D. Nordlund, and O. Stephansson. Technical note, a 3-d constitutive model for rock joints with anisotropic friction and stress dependency in shear stiffness. *International journal of Rock Mechanics and Mining Science*, 31 (2):173–178, 1994.

[41] J. W. Ju. On energy-based coupled elastoplastic damage theories:constitutive modeling and computational aspects. *International Journal of Solid and Structures*, 25(7):803–833, 1989.

[42] Lasar Kachanov. *Introduction to continuum damage mechanics*, volume 10. Springer, 1986.

[43] Nitika Kalia and Vemuri Balaktaiah. Modeling and analysis of wormhole formation in reactive dissolution of carbonate rocks. *Chemical Engineering Science*, 62:919–928, 2007. doi: 10.1016/j.ces.2006.10.021.

[44] Nitika Kalia and Vemuri Balaktaiah. Effect of medium heterogeneities on reactive dissolution of carbonates. *Chemical Engineering Science*, 64:376–390, 2009.

[45] P.S. Lang, A. Paluszny, and R. W. Zimmerman. Permeability tensor of three-dimensional fractured porous rock and comparison to trace map predictions. *Journal of Geophysical Research: Solid Earth*, 119:6288–6307, 2014.

[46] Ming. Liu, Scicheng. Zhang, and Jianye Mou. Wormhole propagation behavior under reservoir condition in carbonate acidizing. *Transp Porous Med*, 2012. doi: 10.1007/s1124 2-012-0084 -z.

[47] J. Lubliner. *Plasticity Theory*. Macmillan, 1990.

[48] D. R. McDuff, C. E. Shuchart, S. K. Jackson, D. Postl, and J. S. Brown. Understanding wormholes in carbonates: Unprecedented experimental scale and 3-d visualization. In *SPE 134379*, September 2010. The paper presented at the SPE Annual Technical Conference and Exhibition in Florence, Italy.

[49] E. S. Minkoff, M. C. Stone, and G. Arguello. Staggered in time coupling of reservoir flow simulation and geomechanical deformation: Step 1-one way coupling. In *SPE 51920*, February 1999. presented in SPE Reservoir Simulation Symposium in Houston.

[50] S. E. Minkoff, C. M. Stone, E. Bryantc, M. Peszynskac, and F. M. Wheelerc. Coupled fluid flow and geomechanical deformation modeling. *Journal of Petroleum Science and Engineering*, 38:37–56, 2003.

[51] M. Nassir, A. Settari, and R. Wan. Modeling shear dominated hydraulic fracturing as a coupled fluid-solid interaction. In *SPE 131736*, pages 8–10, 2010.

[52] Mohammad Nassir. *Geomechanical Coupled Model of Shear Fracturing in Non-Conventional Reservoirs*. PhD thesis, University of Calgary, 2013.

[53] M. Oda. Permeability tensor for discontinuous rock masses. *Géotechnique*, 35(4):483 495, 1985.

[54] M Ortiz and JC Simo. An analysis of a new class of integration algorithms for elastoplastic constitutive relations. *International Journal for Numerical Methods in Engineering*, 23(3):353–366, 1986.

[55] Jose G. Osorio, Her-Yuan Chen, and Lawrence W. Teufel. A two-domain, 3d, fully coupled fluid-flow geomechanical simulation model for reservoirs with stress-sensitive mechanical and fluid-flow properties. In *SPE 47397*, July 1998. presented at SPE Rock Mechanics in Petroleum Engineering, Trondheim.

[56] Frederic Pallet. *Strength and Deformability of Jointed Rock Masses Reinforced by Rock Bolts*. PhD thesis, Swiss Federal Institute of Technology-Lausanne-Switzerland, 1994.

[57] M. K. R. Panga, M. Ziauddin, and V. Balaktaiah. Two-scale continuum model for simulation of wormholes in carbonate acidization. *AIChE Journal*, 51(12): 3231–3248, 2005. doi: 10.1002/aic.10574.

[58] Mohan K.R. Panga, V. Balaktaiah, and M. Ziauddin. Modeling, simulation and comparison of model for wormhole formation during matrix stimulation of carbonates. In *SPE 77369*, 2002.

[59] E. Papamichos, M. Brignoli, and F. J. Santarelli. An experimental and theoretical study of a partially saturated collapsible rock. *Mechanics of Cohesive-frictional Materials*, 2(3):251–278, 1997.

[60] Bertold Plischke. Internal report. Technical report, ISAMGEO GmbH, 2010.

[61] M. David Potts and Lidija Zdravković. *Finite element Analysis in geotechnical engineering Theory*. Thomas Telford Publishing, 1999.

[62] M. Quintard and S. Whitaker. Dissolution of an immobile phase during flow in porous media. *Ind. Eng. Chem. Res.*, 38:833–844, 1999.

[63] F. Rafeh, H. Mroueh, and S. Burlon. Equivalent continuum model accounting for anisotropy in chalk by means of embedded joint sets. In *The 14th International Conference of the International Association for Computer Methods and Advances in Geomechanics, Kyoto, Japan.*, 2014.

[64] R. Risnes and O. Flaageng. Mechanical properties of chalk with emphasis on chalk-fluid interactions and micromechanical aspects. *Oil and Gas Science and Technology-Rev. IFP*, 54(6):751–758, 1999.

[65] MR Salari, S Saeb, KJ Willam, SJ Patchet, and RC Carrasco. A coupled elastoplastic damage model for geomaterials. *Computer methods in applied mechanics and engineering*, 193(27):2625–2643, 2004.

[66] B Singh. Continuum characterization of jointed rock masses, part 1-the constitutive equations. *International journal of Rock Mechanics and Mining Science*, 10:311–335, 1973.

[67] B Singh. Continuum characterization of jointed rock masses, part 2-significance of low shear modulus. *International journal of Rock Mechanics and Mining Science*, 10:337–349, 1973.

[68] B. B. S. Singhal and R. P. Gupta. Fractures and discontinuities. *Applied Hydrogeology of Fractured Rocks*, 2010.

[69] T. David Snow. Anisotropic permeability of fractured media. *Water Resources Research*, 5(9):1273–1289, 1969.

[70] Karl Terzaghi. *Theoretical Soil Mechanics*. John Wiley and Sons, 1943.

[71] David Tran, Antonin Settari, and Long Nghiem. New iterative coupling between a reservoir simulator and a geomechanics module. In *SPE-78192*, October 2002. presented at SPE/ISRM Rock Mechanics Conference, Irving.

[72] M. Ziauddin, V. Balaktaiah, and M. K. R. Panga. Two-scale continuum model for simulation of wormholes in carbonate acidization. *AIChE Journal*, 51(12): 3231–3248, 2005.

[73] R. W. Zimmerman. Coupling in poroelasticity and thermoelasticity. *International Journal of Rock Mechanics and Mining Sciences*, 37(1):79–87, 2000.